Electronic Theses and Dissertations

Theses, Dissertations, and Major Papers

Summer 7-16-2019

Development of dynamic model and control techniques for microelectromechanical gyroscopes

Md imrul Kaes
University of Windsor

Follow this and additional works at: https://scholar.uwindsor.ca/etd

Development of dynamic model and control techniques for microelectromechanical gyroscopes

By

Md. Imrul Kaes

A Thesis

Submitted to the Faculty of Graduate Studies

through the Department of Mechanical, Automotive & Materials Engineering

in Partial Fulfillment of the Requirements

for the Degree of Master of Applied Science

at the University of Windsor.

Windsor, Ontario, Canada

2019

Development of dynamic model and control techniques for microelectromechanical gyroscopes

by

Md. Imrul Kaes

APPROVED BY:

_____

G. Kabir

Department of Mechanical, Automotive & Materials Engineering

_____

N. Zamani

Department of Mechanical, Automotive & Materials Engineering

_____

D. Ting, Co-Advisor

Department of Mechanical, Automotive & Materials Engineering

_____

J. Ahamed, Advisor

Department of Mechanical, Automotive & Materials Engineering

July 16, 2019

DECLARATION OF CO-AUTHORSHIP / PREVIOUS PUBLICATION

I.   Co-Authorship

I hereby declare that this thesis incorporates material that is result of joint research, as follows:

Chapter 4 and 5 of the thesis were co-authored with J. Ahamed. In all cases, primary contributions, experimental designs, data analysis, interpretation, and writing were performed by me and J. Ahamed contributed to the key ideas; D. Ting provided feedback on refinement of ideas and editing of the manuscript.

I am aware of the University of Windsor Senate Policy on Authorship and I certify that I have properly acknowledged the contribution of other researchers to my thesis, and have obtained written permission from each of the co-author(s) to include the above material(s) in my thesis.

I certify that, with the above qualification, this thesis, and the research to which it refers, is the product of my own work.

II.   Previous Publication

This thesis includes 01 original paper that have been previously published/submitted for publication in peer reviewed journals, as follows:

Thesis Chapter	Publication title/full citation	Publication status
Chapter [4]	Md. Imrul Kaes, David S-K Ting, Mohammed Jalal Ahamed " Modeling of Structural and Environmental Effects on Microelectromechanical (MEMS) Vibratory Gyroscopes," Canadian Society for Mechanical Engineers Conference 2018.	Published: Conference: 2018 Canadian Society for Mechanical Engineering (CSME) International Congress

I certify that I have obtained a written permission from the copyright owner(s) to include the above published material(s) in my thesis. I certify that the above material describes work completed during my registration as a graduate student at the University of Windsor.

III.   General

I declare that, to the best of my knowledge, my thesis does not infringe upon anyone's copyright nor violate any proprietary rights and that any ideas, techniques, quotations, or any other material from the work of other people included in my thesis, published or otherwise, are fully acknowledged in accordance with the standard referencing practices. Furthermore, to the extent that I have included copyrighted material that surpasses the bounds of fair dealing within the meaning of the Canada Copyright Act, I certify that I have obtained a written permission from the copyright owner(s) to include such material(s) in my thesis.

I declare that this is a true copy of my thesis, including any final revisions, as approved by my thesis committee and the Graduate Studies office, and that this thesis has not been submitted for a higher degree to any other University or Institution.

ABSTRACT

In this thesis we investigate the effects of stiffness, damping and temperature on the performance of a MEMS vibratory gyroscope. The stiffness and damping parameters are chosen because they can be appropriately designed to synchronize the drive and sense mode resonance to enhance the sensitivity and stability of MEMS gyroscope. Our results show that increasing the drive axis stiffness from its tuned value by 50%, reduces the sense mode magnitude by ~27% and augments the resonance frequency by ~21%. The stiffness and damping are mildly sensitive to typical variations in operating temperature. The stiffness decreases by 0.30%, while the damping increases by 3.81% from their initial values, when the temperature is raised from -40 to 60°C. Doubling the drive mode damping from its tuned value reduces the oscillation magnitude by 10%, but ~0.20% change in the resonance frequency. The predicted effects of stiffness, damping and temperature can be utilized to design a gyroscope for the desired operating condition.

DEDICATION

This work is dedicated to my maker whom by grace, through faith, redeemed my soul and guides my life and to my parents, my wife and kids for their love and support.

ACKNOWLEDGEMENTS

TABLE OF CONTENTS

LIST OF FIGURES

LIST OF TABLES

LIST OF ABBREVIATIONS

2-DOF	Two Degrees-of-Freedom
ADI	Analog Devices Inc.
ASIC	Application-specific integrated circuit
CMOS	Complementary Metal- Oxide Semiconductor
CVD	Chemical Vapor Deposition
DETF	Double-Ended Tuning Forks
DRIE	Deep Reactive Ion Etching
ESD	Electrostatic discharge
HMDS	Hexamethyldisilazane
IC	Integrated Circuit
ICP	Inductively Coupled Plasma
JPL	Jet Propulsion Laboratory
LIGA	Lithography Galvanoformung Abformung
LPCVD	Low-Pressure Chemical Vapor Deposition
MEMS	Microelectromechanical Systems (MEMS)
MUMPs	Multi-User MEMS Processes

PECVD	Plasma Enhanced Chemical Vapor Deposition
PSG	Phosphosilicate Glass
PVD	Physical Vapor Deposition
RIE	Reactive Ion Etching
SOG	Silicon-on-Glass
SOI	Silicon-on-Insulator
TMAH	Tetramethylammonium hydroxide
UV	Ultra Violet
WLP	Wafer-level packaging

NOMENCLATURE

d_0 Demping coefficient at reference temperature of 300 K

d_{xx} Damping coefficient along the drive-axis

d_{xy} Damping error due to manufacturing imperfection

d_{yy} Damping coefficient along the sense-axis

K_0 Stiffness coefficient at reference temperature 300 K

k_{xx} Spring stiffness along the drive-axis

k_{xy} Stiffness error due to manufacturing imperfection

k_{yy} Spring stiffness along the sense-axis

m Proof Mass

Ω_z Absolute angular velocity of the substrate about the z-axis

CHAPTER 1:   INTRODUCTION

A gyroscope is a device mounted on a frame used for measuring or maintaining orientation and angular velocity if the frame is rotating. It is a sensing device that measures the angular rate of an object [1]. A conventional spinning wheel gyroscope is a spinning top combined with a pair of gimbals. The first known device similar to a gyroscope was introduced by John Serson in 1743 [2]. Johann Bohnenberger of Germany, first used a device like an actual gyroscope in 1816 who first wrote about it in 1817 [3]. Foucault gave this device a modern name (Greek skopeein, to see) the Earth's rotation (Greek gyros, circle or rotation) [4]. German inventor Hermann Anschütz-Kaempfe patented the first functional gyrocompass in 1904 [5]. At the beginning of 20th century other devices started to use gyroscopes [6]. Military use of gyroscope has been started widely after the miniaturization technique has been invented [7].

1.1   Applications of MEMS Gyroscopes

Because of wide availability of motion, vibration and shocks, there is almost no place where inertial sensors are not found. Though the initial interest on gyroscope started with navigation, telescope, imaging system and antennas, it is has now spread everywhere including automotive industry because of its low cost, high reliability and possibility of mass production [8].

Navigation: Inertial navigation sensors (INS) now a days are used to figure out the position, velocity and attitude of the vehicle. INS is used for land vehicle navigation

systems for non-holonomic constraints and using odometer measurements. Pedestrian navigation systems using biomechanics help many disable people walking. Inertial sensors are widely used for identifying the occurrence of steps which helps estimating the distance and direction in which the steps were taken.

Automotive: Recent cars use MEMS accelerometers for airbag deployment systems which is further used for detecting a rapid negative acceleration of the vehicle, finding out if a collision is happened, and calculating the severity of the collision. MEMS gyros and accelerometers are also used in electronic stability control systems to keep the car towards its intended direction. MEMS gyroscope is also used in conditions that cause discomfort for drivers and passengers, harshness and monitoring of noise.

Industrial: In industry, accelerometer has wide application specially in monitoring vibration. Bearing fault in rotating equipment such as turbines, pumps, fans, rollers, compressors, and cooling towers, gear failure, reduce downtime are some major applications of MEMS gyroscope.

Consumer Products: The miniaturization of accelerometers and gyroscopes revolutionized the industry of game controllers, mobile phones, cameras, and other personal electronic devices. Other popular applications are sport and healthy lifestyle, gesture recognition, orientation sensing, motion input, image stabilization and fall detection. Objects in space can be moved with accelerometer embedded wireless mouse.

Inertial sensor embedded cameras are used for image stabilization. Fall detection feature now has become common for many consumer products by the virtue of accelerometer.

Sport: Today's pedometer is a gift of modern accelerometer which is the simplest form of step counter. Inertial sensors contributed a lot to the technology of motion analysis specially javelin, ski jumping and figure skating. Now we can easily detect not only human movement but also the movement of different parts of the body and these data are used in medical and virtual environments.

1.2   Types of Gyroscopes

Several kinds of gyroscopes are available in the market. Most common ones are mechanical gyroscope, optical gyroscope and microelectromechanical gyroscope.

Mechanical Gyroscopes

In this kind of gyroscope, a mass called spinning mass, spins around its axis. The special feature of it is that when the mass spins it tries to stay parallel to itself and to oppose any attempt to change its orientation. Léon Foucault discovered this mechanism. Precession and nutation are few of the many physical phenomena that mechanical gyroscope shows. Figure 1 shows typical mechanical gyroscope. In mechanical gyroscope, proof mass tries to remain in its angular position and when an external torque is introduced, it experiences a precession motion which is normal to the applied torque.
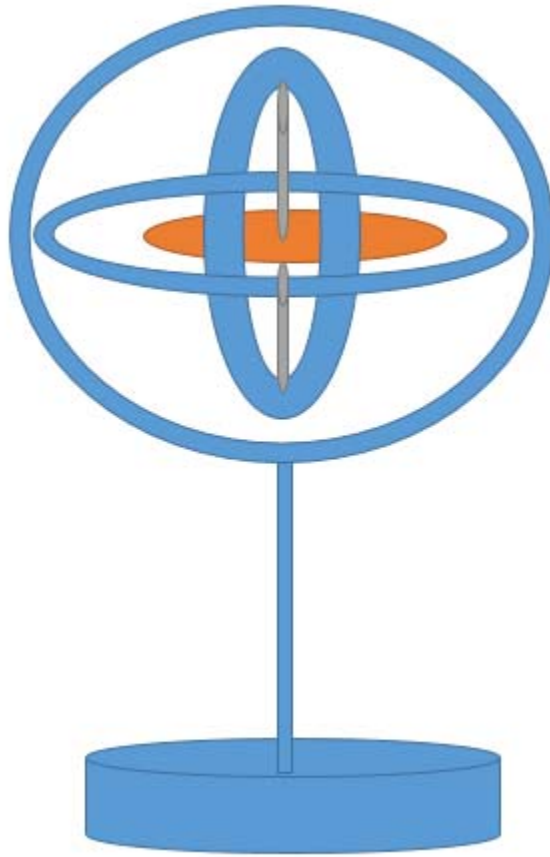
Figure 1: Mechanical Gyroscope

Optical Gyroscopes

The basic feature of optical gyroscope is the laser cavity in the light path which augment the Signac effect. The basic principle of the optical gyroscope shows in Figure 2. An active source of laser output is used in a confined cavity. The cavity has reflecting mirrors. A pair of laser beam is directed at the same time in two opposite directions. When the resonator spins, because of Signac effect two lasers experience different cavity length

and therefore, frequency difference occurs. Time varying phase shift appears due to this frequency difference and number of beat period can be calculated from it. From this beat period, angular increment can be easily found out.
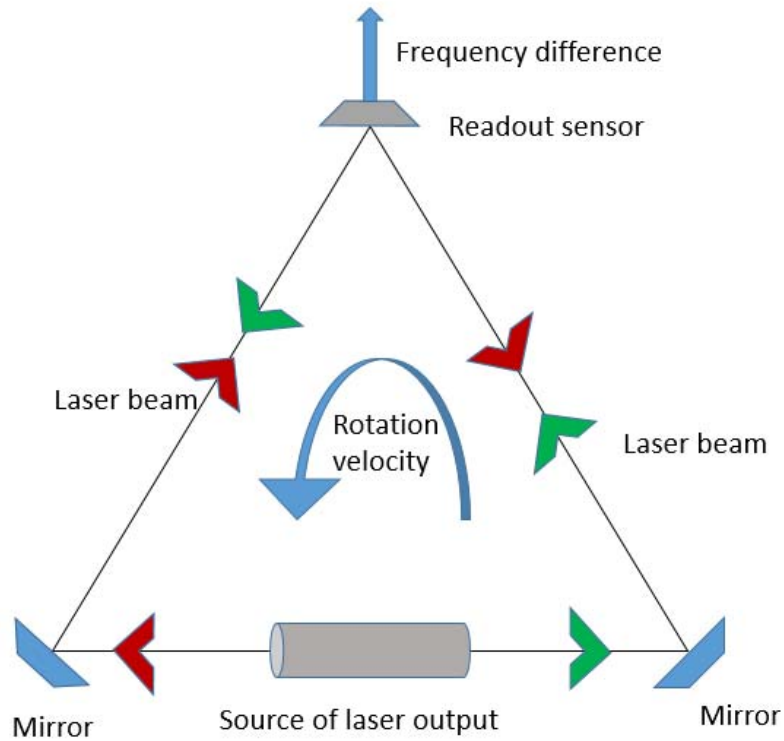
Figure 2: Optical gyroscope

Microelectromechanical (MEMS) gyroscopes

MEMS gyroscopes utilize vibrating structure as a sensing element for identifying the angular velocity. They consist of bearings. When the proof mass vibrates and given a rotation, a force named Coriolis introduced which transfer energy between two vibration modes. The Coriolis force is proportional to the angular velocity. Figure 3 shows typical MEMS vibratory gyroscope.
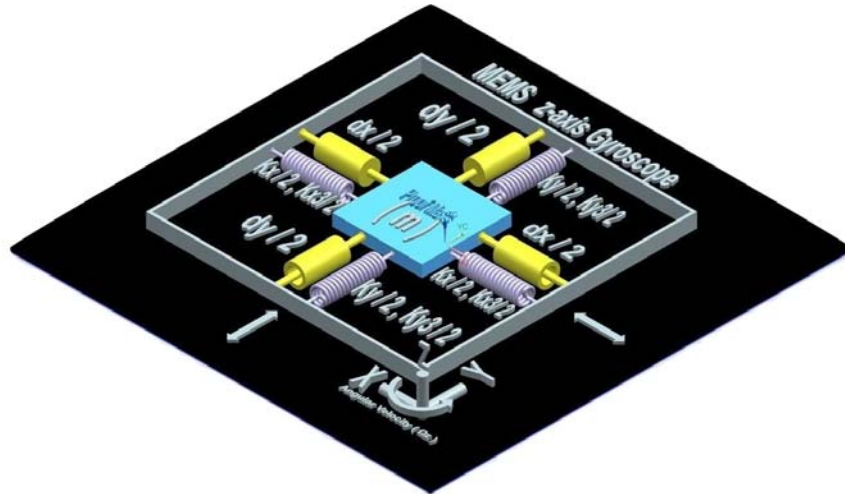
Figure 3: MEMS Vibratory gyroscope
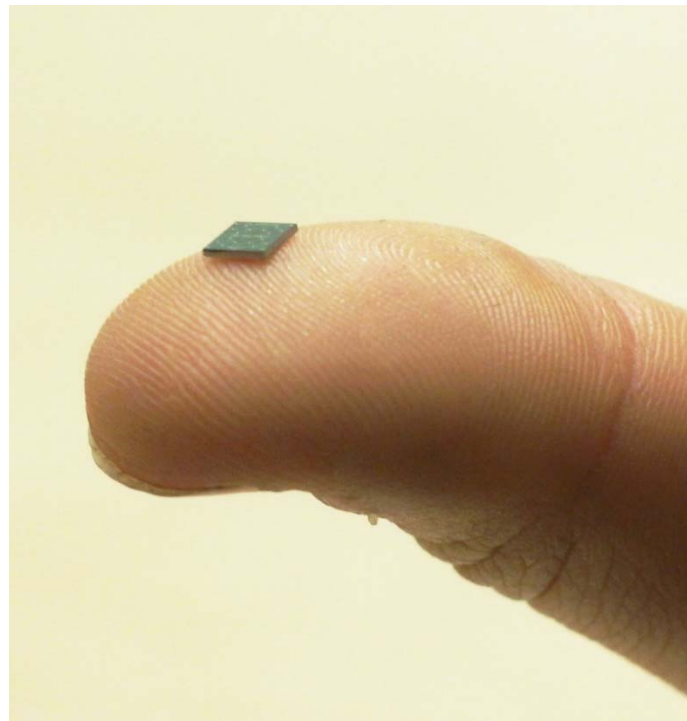
Figure 4:   MEMS Gyroscope Developed at Micro Nano Mechatronics Lab at

University of Windsor

1.3   Gyroscope Performance Specifications

The performance specifications of gyroscope are mentioned in the IEEE Standard Specification Format Guide and Test Procedure for Coriolis Vibratory Gyros [10]. The following is a summary of important specifications [11].

Scale factor: It is the ratio of output change in respect to input change which is measured in mV/°/second.

Nonlinearity: It is the shift from the line which represents the relationship between inputs and outputs.

Scale factor temperature and acceleration sensitivity: It is the drift in scale factor which occurs due to a change in steady state operating temperature and a constant acceleration.

Bias: It is the mean over a specific time of gyroscope output which is quantified in specific operating conditions. Bias is measured in °/sec or °/hr.

Environmentally sensitive drift rate: It depends on environmental parameters which includes temperature hysteresis, acceleration sensitivity, temperature sensitivity, temperature gradient sensitivity, vibration sensitivity etc.

Shock Resistance: It is the maximum shock that the operating or non-operating equipment can stand before failure [12]. This shock resistance are determined during testing and calibration. [13] Typical performance grades for gyroscopes are shown in Table 1.

Table 1: Typical performance grades for gyroscopes

Typical Performance Grade				
		Performance Grades		
Performance Parameter	Performance Units	Inertial	Intermediate	Moderate
Maximum Input	Deg/h	$10^2 - 10^6$	$10^2 - 10^6$	$10^2 - 10^6$
	Deg/s	$10^{-2} - 10^2$	$10^{-2} - 10^2$	$10^{-2} - 10^2$
Scale factor	Part/part	$10^{-6} - 10^{-4}$	$10^{-4} - 10^{-3}$	$10^{-3} - 10^{-2}$
Bias stability	Deg/h	$10^{-4} - 10^{-2}$	$10^{-2} - 10$	$10 - 10^2$
	Deg/s	$10^{-8} - 10^{-6}$	$10^{-6} - 10^{-3}$	$10^{-3} - 10^{-2}$
Bias drift	Deg/√h	$10^{-4} - 10^{-3}$	$10^{-2} - 10^{-1}$	$1 - 10$
	Deg/√s	$10^{-6} - 10^{-5}$	$10^{-5} - 10^{-4}$	$10^{-4} - 10^{-3}$

1.4   Vibratory Gyroscope Principle

In vibratory gyroscope the proof mass can freely vibrate in the drive and the sense directions. The proof-mass is accelerated in the drive direction by a sinusoidal force introduced from outside. When the gyroscope is given an angular rotation, a sinusoidal Coriolis force at the frequency of drive mode oscillation is introduced in the sense direction. The Coriolis force makes the proof-mass to oscillate in the sense direction and the displacement due to this is detected by the detection electrodes.
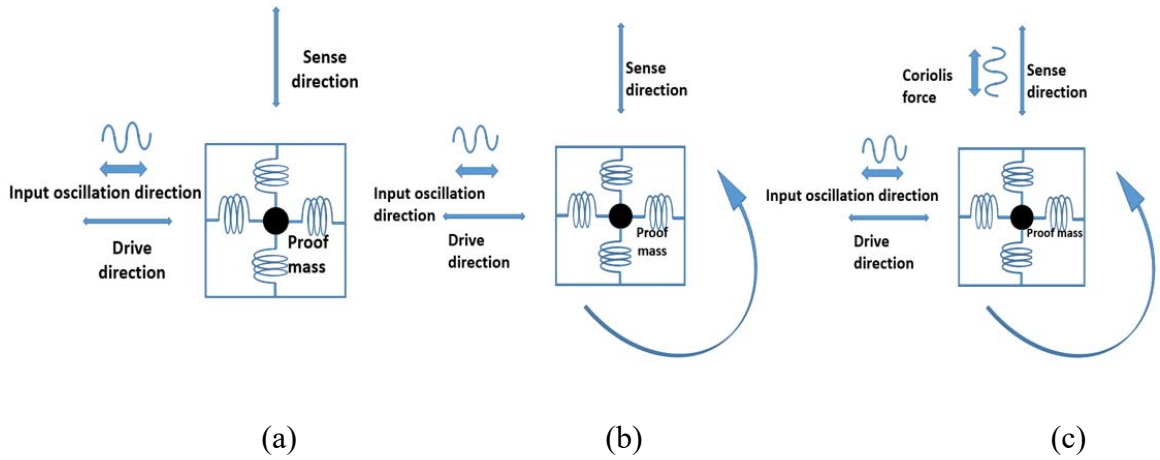
Figure 5: The vibratory gyroscope principle (a) (b) (c)

1.5   Literature review:

Microelectromechanical systems (MEMS) inertial sensors like accelerometers and gyroscopes are the most popular MEMS technology till now. With the rapid development of fabrication technology, the cost and size of MEMS are decreasing and the power is increasing which is augmenting new uses in automotive, aerospace, biomedical and consumer electronics. MEMS vibratory gyroscopes find its wide application in detecting the angular rate of an object in respect of a reference frame [14] [15] [16] [17]. A proof mass is used to calculate the angular rotation [2]. The Coriolis Effect plays a key role for measuring this rate of rotation [18]. Because external disturbances, it becomes almost impossible to get the accurate value of resonant frequencies which reduces the performance of gyroscope. Therefore, proper design and optimization of influencing parameters are necessary. Finite element analysis modeling, analytical modeling and simplified lumped

parameter modeling can be helpful to design a robust system [4]. These methods are robust, flexible and accurate and can be used with controllers and electronics for better result [5] [19]. In MEMS gyroscopes, manufacturing defects always exist which adversely affect the performance. Robust and efficient controllers are necessary for the compensation [20].

However, quantitative measurement of the individual and combined influence of stiffness, damping and temperature on MEMS gyroscope have not been found in the literature. In this thesis, a lumped-parameter model for predicting the gyroscope performance with the influence of various system parameters such as stiffness, damping and environmental condition (temperature) have been analyzed. The results can be utilized to design a robust high performance gyroscope with efficient controllers.

CHAPTER 2:   OBJECTIVE & METHODOLOGY

This section includes the description of the specific objectives and methods for

(1) The development of a lumped parameter model to capture MEMS vibratory gyroscope dynamics.

(2) The investigation of the effects of temperature, stiffness and damping on the performance of a MEMS vibratory gyroscope. For example, for stiffness 80.98 N/m, damping coefficient 71.62 N s/m and at 300 K temperature resonance frequency is found at 19.4 kHz with magnitude 5.40 dB and amplitude 0.025 μm. Our investigation will focus on what percentage of amplitude, magnitude and resonance frequency change when the values of stiffness coefficient, damping coefficient and temperature are varied with in certain range like stiffness and damping coefficient from half to double, temperature from 270 K to 330 K.

(3) The augmentation of the gyro performance (reduce noise) using advance controller.

There are three primary steps which have been followed in this study:

(1) To develop a model relating to gyroscope vibrational characteristics with temperature, stiffness, proof mass, angular rate and damping.

(2) To perform simulation and experiment to evaluate the effects of temperature, stiffness and damping on gyro performance.

(3) To develop and optimize a controller to enhance gyro performance.

According to the equation of motion, the dynamics of gyroscope have been developed. We assumed that the behavior of the spring is linear. Frequency response curve has been used to compare the effects of varying stiffness, damping and temperature on gyro performance. Frequency response curve shows the comparison between the output and input as a function of frequency. Magnitude is the logarithmic ratio of output and input. The decibel is used for measuring magnitude. If output amplitude is smaller than input, magnitude becomes negative. MATLAB Simulink [21] is used for simulation and computation. As the performance of the MEMS gyroscope is often deteriorated by the effects of time-varying parameters, quadrature errors and external disturbances, we need a controller. After considering advantages and limitations of different controllers, we select a suitable controller to restore distorted output signal.

CHAPTER 3:   MODELING GYROSCOPE DYNAMICS

Typical MEMS vibratory gyroscope consists of a proof mass, spring suspensions, electrostatic actuations and sensing mechanisms. These mechanical arrangements can be considered as a mass, spring, and damper system. In this thesis, only linear vibratory gyroscopes are considered. Figure 3 shows a simplified model of a MEMS gyroscope having two degrees of freedom. Assuming that the proof mass can only move along the x and y plane by making the spring stiffness in the z direction. Considering the angular rate almost constant, the equation of motion of a gyroscope is simplified as follows.

$$m\ddot{x}+d_{xx}\,\dot{x} + (k_{xx} - m\,(\Omega_y{}^2 + \Omega_z{}^2))\,x + m\,\Omega_y\Omega_x\,y\ = u_x + 2m\,\Omega_z\,\dot{y} \qquad (1)$$

$$m\ddot{y}+d_{yy}\,\dot{x} + (k_{yy} - m\,(\Omega_x{}^2 + \Omega_z{}^2))\,y + m\,\Omega_y\Omega_x x\ = u_y - 2m\,\Omega_z\,\dot{x} \qquad (2)$$

Here d_{xy}, k_{xy} are cross damping and cross spring coefficients, Ω is the angular velocity, u_x, u_y are external forces. $2m\,\Omega_z\,\dot{x}$ and $2m\,\Omega_z\,\dot{y}$ are Coriolis forces Equation 1 and Equation 2. According to the assumption only Ω_z, causes a dynamic coupling and due to this $\Omega_x{}^2 \approx \Omega_y{}^2 \approx \Omega_x{}^2\Omega_y{}^2 \approx 0$ has been considered. As manufacturing imperfection will be always there Equation 1 and Equation 2 are modified as Equation 3 and Equation 4 as follows [22]:

$$m\ddot{x}+d_{xx}\,\dot{x} + k_{xx}\,x + k_{xy}\,y + d_{xy}\,\dot{y} = u_x + 2m\,\Omega_z\,\dot{y} \qquad (3)$$

Equation 3 shows the force balance between external force, Coriolis force and acceleration force, stiffness force, cross stiffness force, cross damping force to the drive direction.

$$m\ddot{y} + d_{yy}\dot{y} + k_{yy}\,y + k_{xy}\,x + d_{xy}\,\dot{x} = u_y - 2m\,\Omega_z\,\dot{x} \qquad (4)$$

Equation 4 shows the force balance between external force, Coriolis force and acceleration force, damping force, cross stiffness force, cross damping force to the sense direction.

Manufacturing imperfections are represented with spring and damping terms, k_{xy} and d_{xy}. The drive and sense mode spring and damping are represented by k_{xx}, k_{yy}, d_{xx} and d_{yy} are deterministic [23]. To make the numerical simulation easy, scaling of the equations have been performed. The realization of dimensional control is done by multiplying the dimensionalizing parameters with the scaled terms. q_0 and w_0, are the length and natural resonance frequency respectively and the scaling of Equation 5 and Equation 6 can be done as follows:

$$\ddot{x} + \frac{w_x}{Q_x}\dot{x} + d_{xy}\dot{y} + w^2{}_x x + w_{xy}\,y = u_x + 2\,\Omega_z\,\dot{y} \qquad (5)$$

$$\ddot{y} + \frac{w_y}{Q_y}\dot{y} + d_{xy}\dot{x} + w^2{}_y y + w_{xy}\,x = u_y - 2\,\Omega_z\,\dot{x} \qquad (6)$$

Where Q_x and Q_y are respectively the drive and sense quality factors,

$$w_x = \sqrt{\frac{K_{xx}}{mw^2{}_0}},\ w_y = \sqrt{\frac{K_{yy}}{mw^2{}_0}},\ w_{xy} = \frac{K_{xy}}{mw_0{}^2},\ d_{xy} \leftarrow \frac{d_{xy}}{mw_0},\ \Omega_z \leftarrow \frac{\Omega z}{w_0},\ u_x \leftarrow \frac{u_x}{mq0\ w_0{}^2},\ ,\ u_y \leftarrow \frac{u_y}{mq0\ w_0{}^2}$$

We can describe mathematically the governing equations for typical mode of operation by the following equations:

$$x = X_0 \sin (w_x t) \qquad (7)$$

$$\ddot{y} + \frac{w_y}{Q_y} \dot{y} + w_y{}^2 \, y = u_y - w_{xy} \, x - (d_{xy} + 2 \, \Omega_z) \dot{x} \qquad (8)$$

The negative impact of the cross damping d_{xy} on gyroscope performance has not been considered by many researchers so far. However, its effect should not be underestimated [24]. In reality it is not easy to identify and cover up for all the manufacturing imperfections. One way to get these manufacturing imperfections compensated by creating richer gyroscope dynamics.

Simulation has been done to observe the influence of stiffness, damping and temperature on gyroscope performance to minimize time and cost of expensive trial and error with the actual fabrication cycle [12]. The SIMULINK model (Figure 6) has been developed from the Equation 3 and Equation 4. The following parameters have been used for simulation - proof mass, $m = 0.57e^{-8}$ kg, damping coefficient along the drive-axis, d_{xx} $= 0.429e^{-6}$ N s/m, damping error due to manufacturing imperfection, $d_{xy} = 0.0429e^{-6}$ N s/m, damping coefficient along the sense-axis, $d_{yy} = 0.687e^{-6}$ N s/m, spring stiffness along the drive-axis, $k_{xx} = 80.98$ N/m, stiffness error due to manufacturing imperfection, $k_{xy} = 5$ N/m, spring stiffness along the sense-axis, $k_{yy} = 71.62$ N/m, angular velocity, $\Omega_z = 5$ rad/s are considered [23].
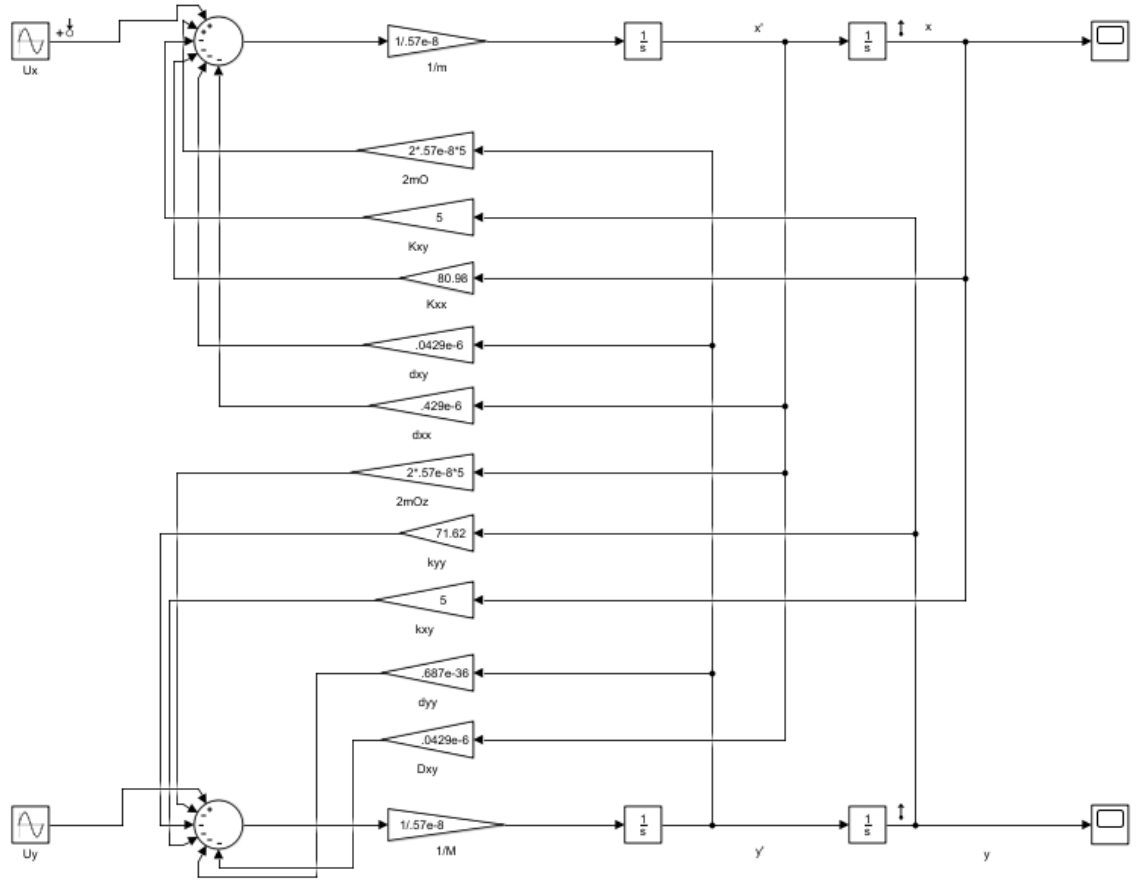
Figure 6: SIMULINK model of gyroscope

In this SIMULINK model we apply a sinusoidal voltage as an input as an external force u_x and sense the displacement in both in drive (x) and sense (y) directions. As it is a second order equation, we integrate acceleration and velocity to get the displacements. For stiffness, damping, cross stiffness, cross damping, proof mass, angular velocity, tuned values have been used from the literature. To balance, the forces are connected to nodes with appropriate signs. Directions are shown with arrows. Multiplications are shown with triangles with values inside. Here "Sum 1 node" is actually constructing Equation 3 which is balancing $m\ddot{x}$, $d_{xx}\dot{x}$, $k_{xx}\,x$, $k_{xy}\,y$, $d_{xy}\dot{y}$, u_x, $2m\,\Omega_z\dot{y}$. On

16

the other hand "Sum 2 node" is constructing Equation 4 which is balancing $m\ddot{y}$, $d_{yy}\dot{y}$, k_{yy} y, k_{xy} x, $d_{xy}\dot{x}$, u_y, $2m\,\Omega_z\,\dot{x}$. For integration we use "Integrator" and to watch the output we added "Scope" in the model. We get the Bode-Plot by setting the frequency range from 1 kHz to 100 kHz with linearly spaced 10,000 frequencies. To smooth the curve 100 moving average method has been used.

CHAPTER 4:   MODEL RESULTS

Parameters have been varied on the model in Matlab SIMULINK, developed in chapter 2. The parameters varied are mass, angular rate, spring stiffness, damping coefficient and temperature which influence the output performance of gyroscope. Thus, the objective of the simulation is to quantify the effects of these parameters. These parameters are very vital for equipment where the resonance frequency is the principal factor in determining the gyro performance [25].

After sweeping the simulation with the frequency range of 1 kHz to 60 kHz (Figure 7), the resonance frequency is found at around 19.4 kHz. So, for better focusing, the frequency range is restricted from 10 kHz - 30 kHz for other comparisons.
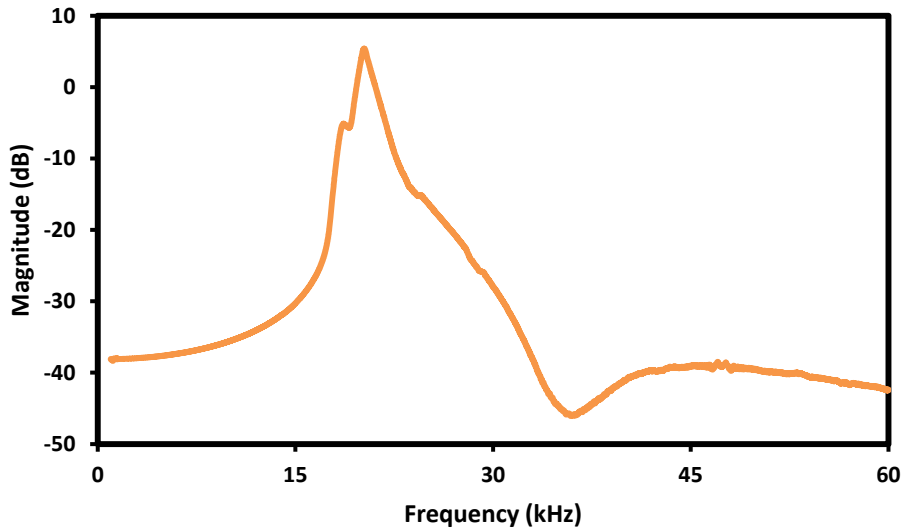

Figure 7: Frequency-Response Curve

The spring stiffness and damping coefficient are varied from half to double of their nominal values. The temperature is varied from -40^0 C to 60^0 C to observe the temperature effect on stiffness, damping coefficient and on sensing magnitude. For the simulation model, the nominal values for the proof mass, stiffness, and damping are extracted from the literature reported in [26].

4.1 Effect of stiffness (Drive Mode) on resonance frequency

Suspension beam along drive and sense direction provides the stiffness necessary in each direction. Keeping the k_{yy} value constant at 71.62 N/m, k_{xx} is varied from 50% (normalized value "0.5") to 150% (normalized value "1.5"). The normalized value of tuned reference stiffness (80.98 N/m) is considered as "1". It is observed that magnitudes at resonance frequencies show linear decreasing trend (Figure 9) and amplitudes decrease (Figure 8) as stiffness increases. However, decreasing the stiffness creates phase lag and distortion in output response.

$$m\ddot{x} + d_{xx}\,\dot{x} + \mathbf{k_{xx}}\,x + k_{xy}\,y + d_{xy}\,\dot{y} = u_x + 2m\,\Omega_z\,\dot{y} \qquad (9)$$

In the following figures, "1" means reference stiffness (80.98 N/m), "1.5" means stiffness has been increased by 50%. It is observed that if stiffness goes up by 50%, resonance frequency goes up by 21% and magnitude goes down by 27%.
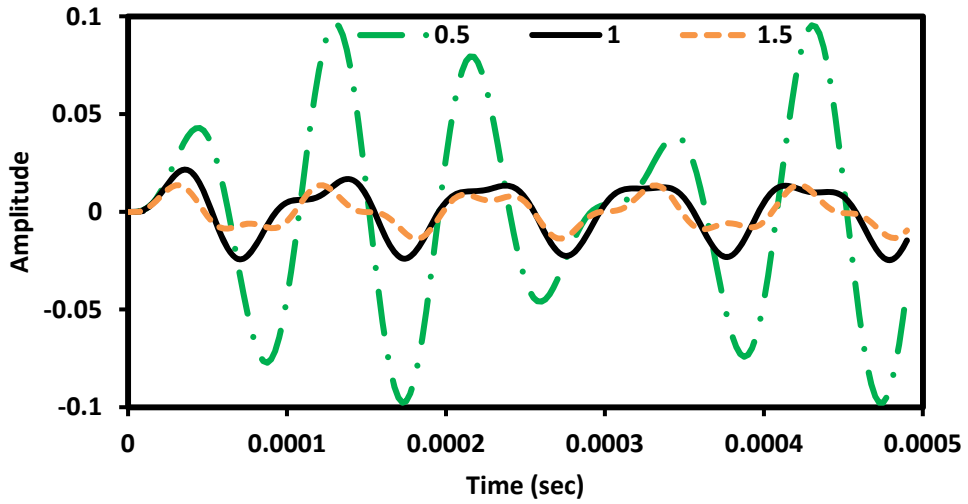
Figure 8: Effect of drive mode stiffness on output sense (sense mode stiffness is constant)
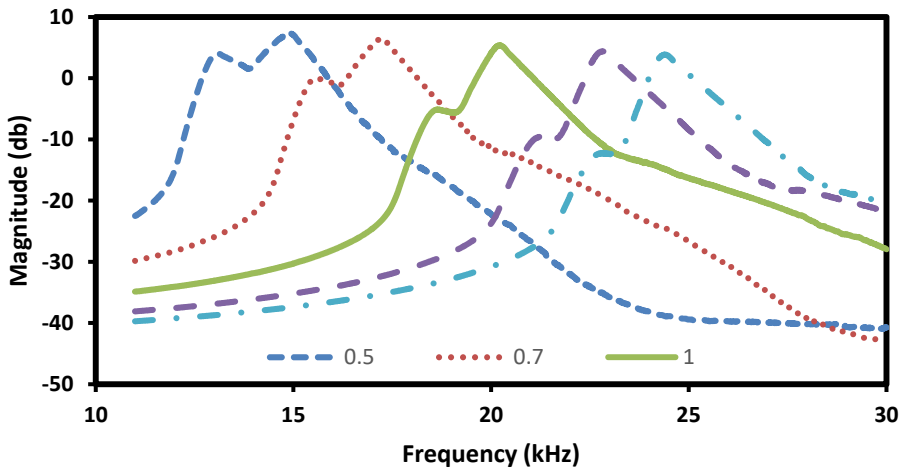

Figure 9: Effect of drive mode stiffness on resonance frequency and its magnitude

4.2 Effect of stiffness (Sense Mode) on resonance frequency

In Figure 10 it has been observed that resonance frequency doesn't change that much with the change of sense mode stiffness. In the Figure 10, "1" means reference stiffness (71.62 N/m), "1.5" means stiffness has been increased by 50%.

$$m\ddot{y}+d_{yy}\,\dot{y}+\mathbf{k_{yy}}\,y+k_{xy}\,x+d_{xy}\,\dot{x}=u_y+2m\,\Omega_z\,\dot{x} \qquad (10)$$

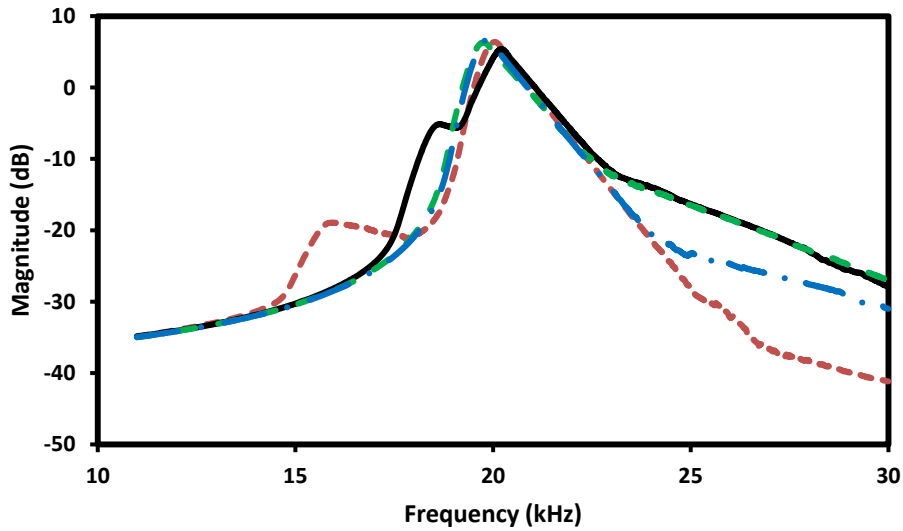Figure 10: Effect of sense mode stiffness on resonance frequency

4.3 Effect of stiffness (both Drive Mode and Sense Mode) on resonance frequency

Variation in stiffness (k_{xx} and k_{yy}) along both axes decreases magnitudes at resonance frequencies and resonance frequencies shift towards higher frequencies (Figure 11) and amplitudes also decreases as stiffness increases (Figure 12). In the Figure 11, "1"

means reference stiffness (80.98 N/m, 71.62 N/m), "1.5" means stiffness has been increased by 50%.
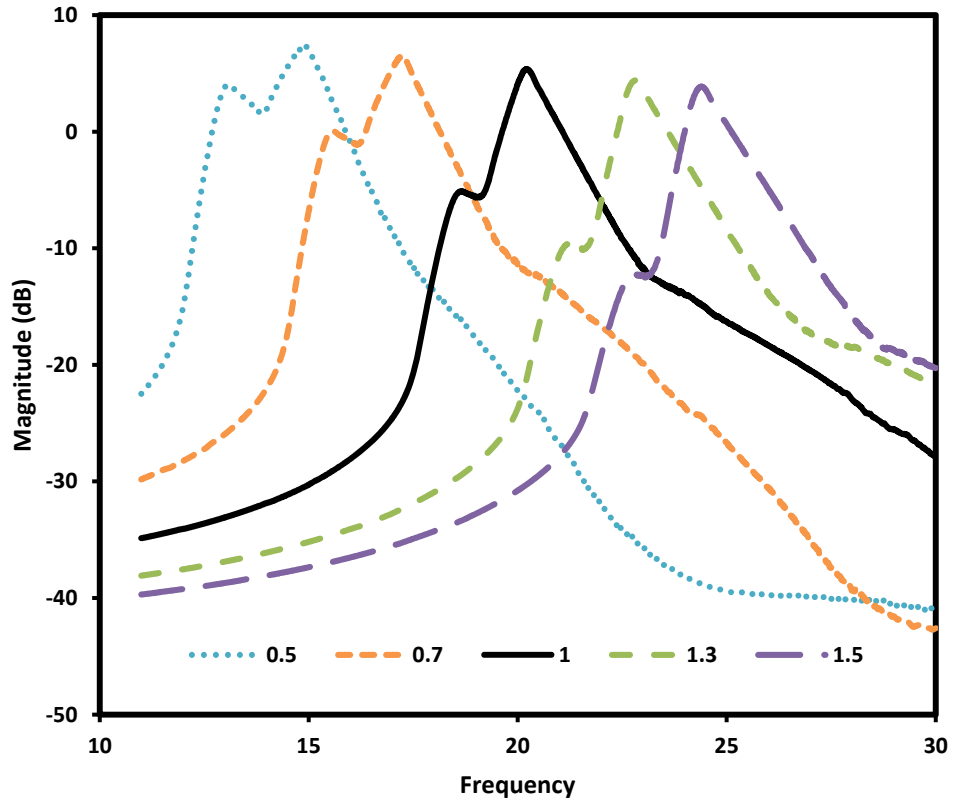

Figure 11: Combined effect of drive mode stiffness and sense mode stiffness on magnitude
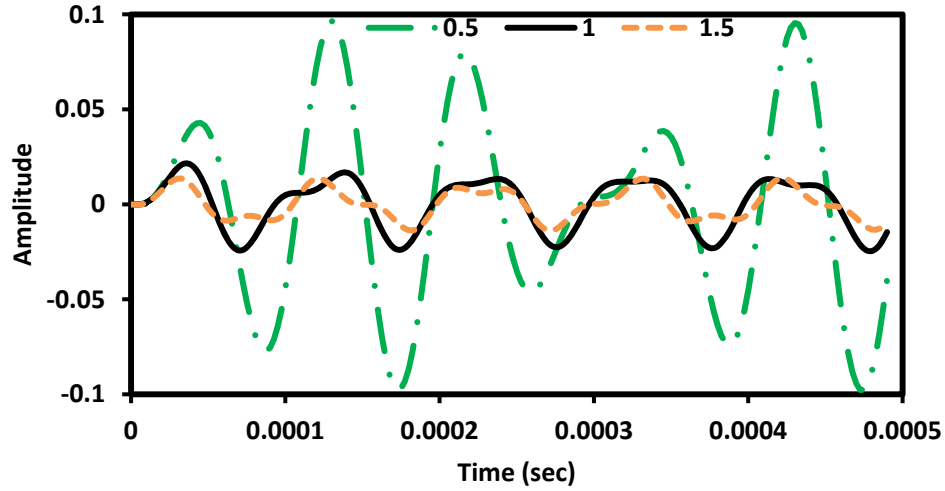
Figure 12: Effect of drive mode stiffness and sense mode stiffness on output sense

4.4 Effect of damping (Drive Mode) on resonance frequency

$$m\ddot{x} + d_{xx}\,\dot{x} + k_{xx}\,x + k_{xy}\,y + d_{xy}\,\dot{y} = u_x + 2m\,\Omega_z\,\dot{y} \qquad (11)$$

Here, damping along the drive axis is varied (Figure 13). When damping increases to double, magnitude of resonance goes down by 10% and resonance frequency itself goes down by 0.16%. It is obvious from the Figure 13 that the resonance frequencies do not change that much but the steepness of the slope decreases as drive mode damping increases after resonance frequencies. Here, "1" means reference damping ($0.429e^{-6}$ N s/m), "0.5" means damping has been reduced by 50%, "2" means damping has been increased to double.
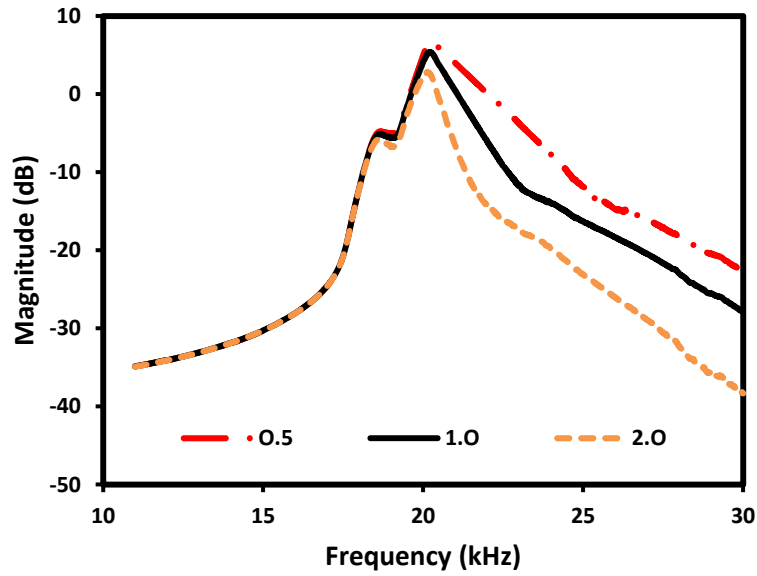
23

Figure 13: Effect of drive mode damping on resonance frequency

4.5   Effect of temperature variation on stiffness and damping

One key disadvantage of MEMS gyrosocpe is its high thermal sensitivity. The frequency of oscillation drifts with temperture. Temperature variation mainly affects the stiffness and damping of the supporting beams. Here investigation on the temperature sensitivity for stiffness and damping is done. The variation of stiffness with temperature can be modeled using simplified linear relationship of [4]

$$K(T) = K_0(1 - k\Delta T) \tag{12}$$

where K_0 is the stiffness coefficient at reference temperature 300 K and k = 70 ppm. Variation of damping coefficient with temperature can be modeled as [4]

$$d(T) = d_0 . 1.28^{\ln(\frac{T}{300})} \tag{13}$$

Where T is temperature in K , d_0 is demping coefficient at reference temperature of 300 K.

Magnitude   shows positive increasing trend with the increase of temperature when stiffness and temperature relationship shows linear behaviour. The damping coefficient within normal operating temperature range   shows decreasing trend as temperature increases (Figure 14).

4.6   Effect of temperature variation on stiffness coefficient

When the temperature increases, the atoms of the object gain significant amount of Kinetic energy. Kinetic energy is a measure of the ability to move. This causes atoms to move apart causing an increase in the area. When the area increases, the stress (Force / Area) decreases. Young's modulus E = Stress / Strain. As the numerator falls, the value of E also falls. This is why Young's modulus decreases with increase in Temperature. As spring stiffness is related to Young's modulus, it decreases as the temperature increases.

When the temperature is raised from -40°C to 60°C, stiffness goes down by 0.70 %.

Figure 14: Relationship between temperature and stiffness

When the stiffness changes by 0.70 %, magnitude changes by 0.378 %.
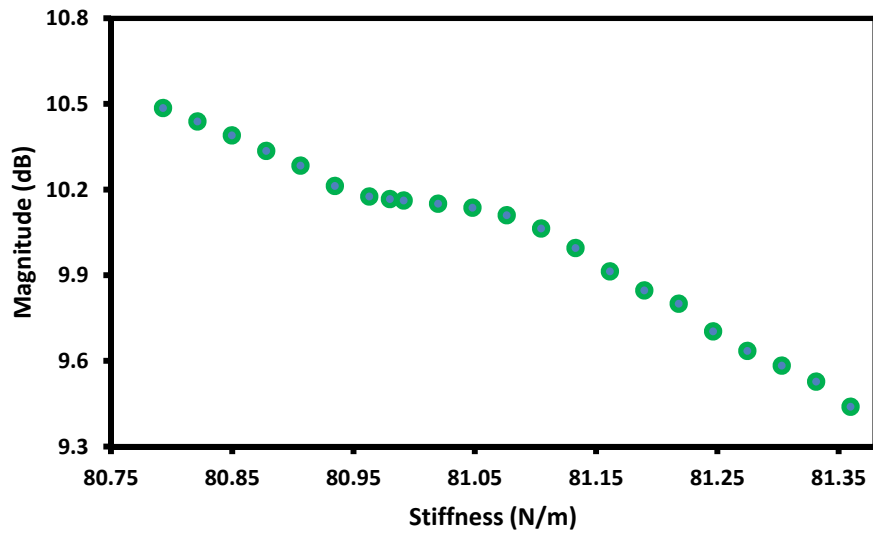
Figure 15: Relationship between stiffness and magnitude when temperature changes

4.7   Effect of temperature variation on damping coefficient

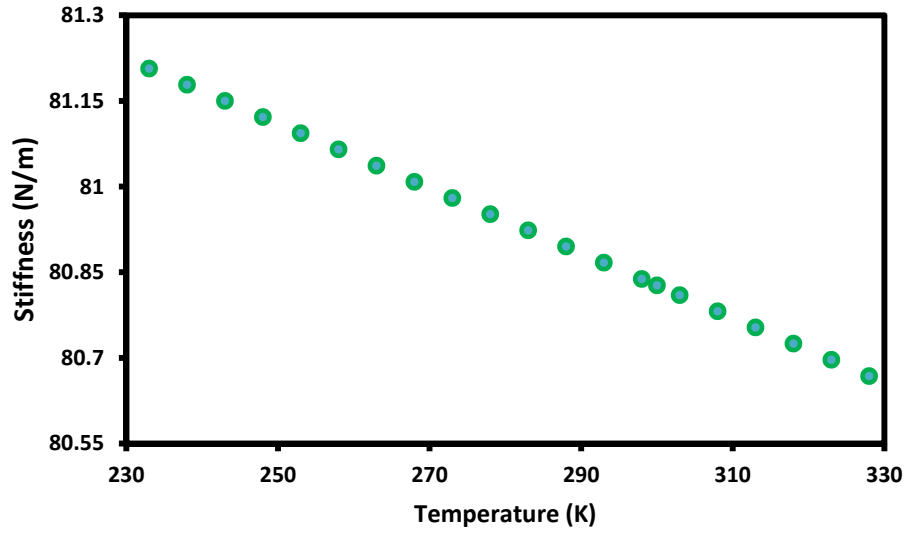When the temperature is raised from -40°C to 60°C, damping is going up by 9.22 %.
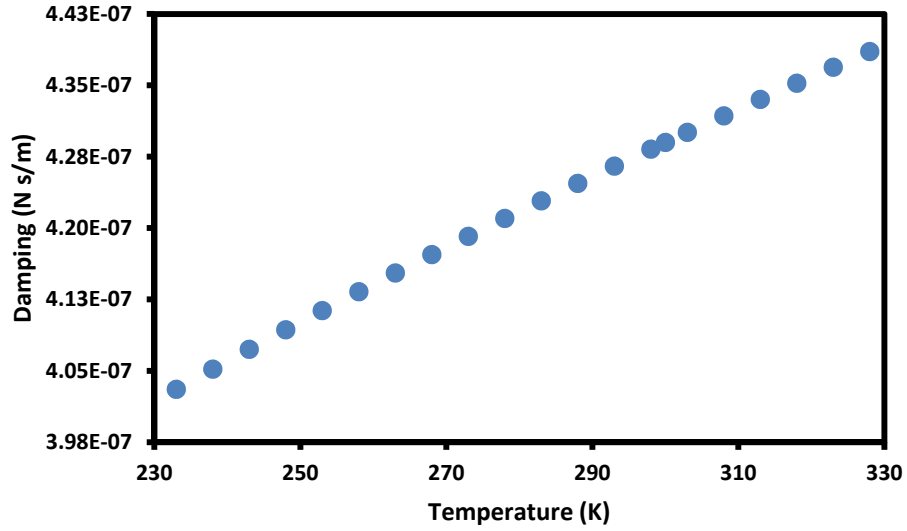
Figure 16: Relationship between temperature and damping

When the Damping changes by 9.22 %, magnitude changes by 0.92 %.
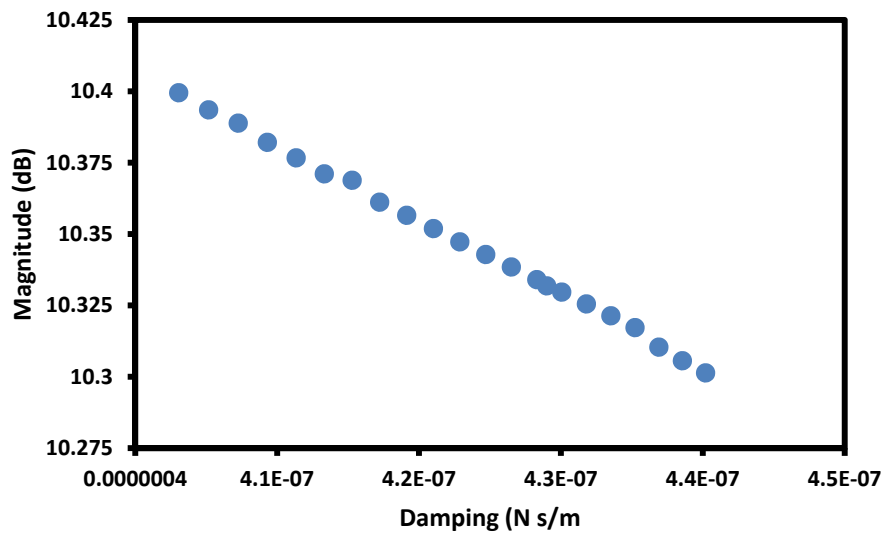
Figure 17: Relationship between damping and magnitude when temperature changes

4.8   Effect of mass variation on resonance frequency
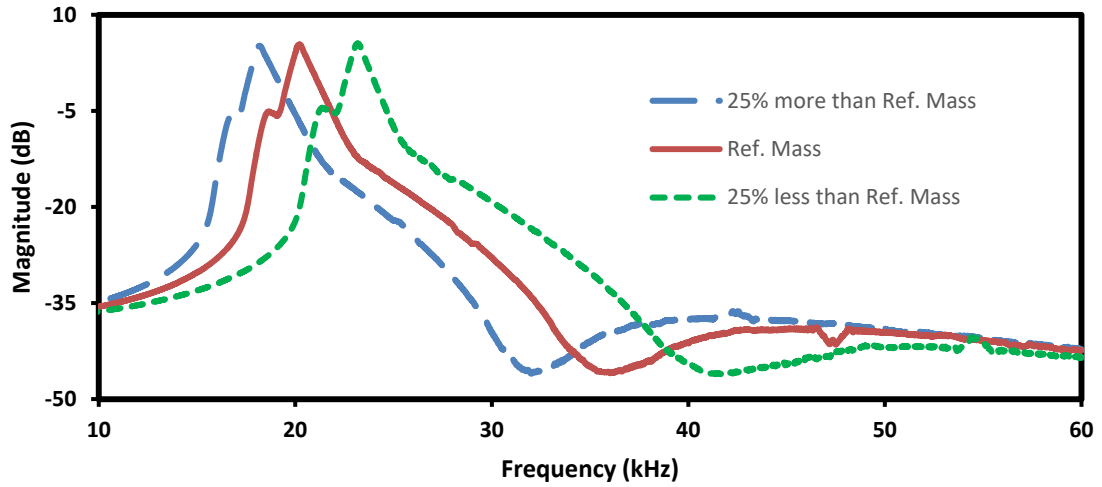
Figure 18: Effect of mass variation on response curve

Here, m is varied from 75% (normalized value 0.75) to 125% (normalized value 1.25). The normalized value of tuned reference mass ($0.57e^{-8}$ kg) is considered as 1. It is observed that magnitudes at resonance frequencies show linear increasing trend (Figure 18) as mass decreases.

$$\mathbf{m}\ddot{x} + d_{xx}\,\dot{x} + k_{xx}\,x + k_{xy}\,y + d_{xy}\,\dot{y} = u_x + 2m\,\Omega_z\,\dot{y} \qquad (11)$$

It is observed that if mass goes down by 50%, magnitude goes down by 5%.

4.9   Effect of angular rate variation on sense frequency
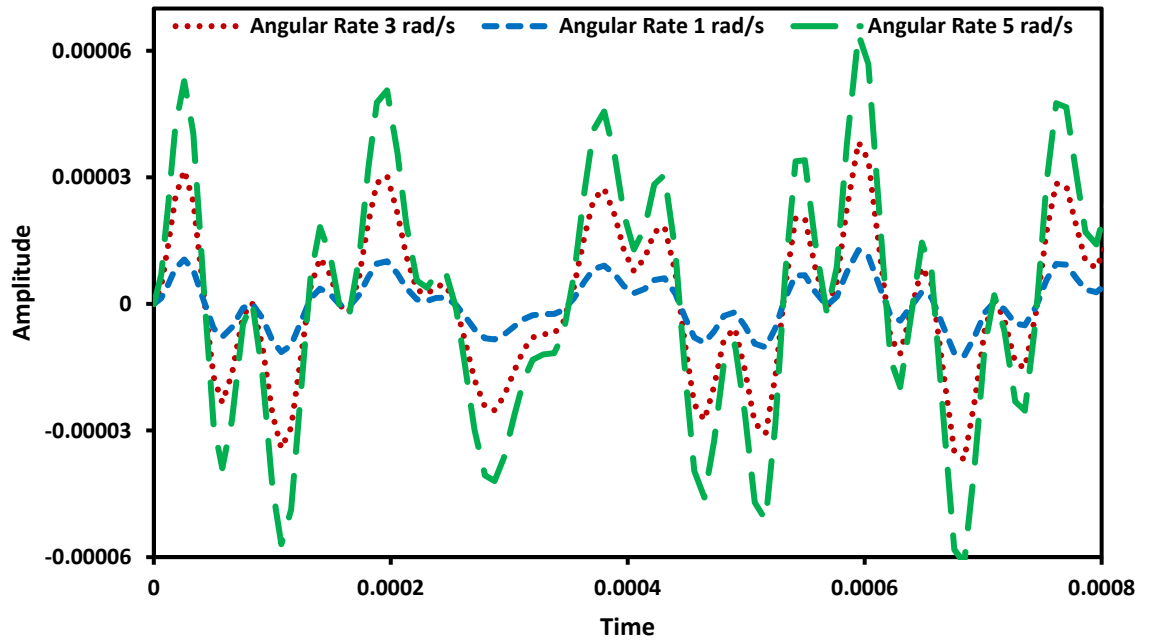
Figure 19: Effect of angular rate variation on output signal

$$m\ddot{x} + d_{xx}\,\dot{x} + k_{xx}\,x + k_{xy}\,y + d_{xy}\,\dot{y} = u_x + 2m\,\mathbf{\Omega_z}\,\dot{y} \qquad (11)$$

Angular rate has an impact on the performance of gyroscope output. As it is observed in Figure 19 that with the variation of angular rate, amplitude of the sense output varies significantly. It has been found that at 1 rad/s angular rate maximum amplitude is 0.0023, at 3 rad/s angular rate maximum amplitude is 0.0070 and at 5 rad/s angular rate maximum amplitude is 0.0117 which clearly showing an increasing trend.

CHAPTER 5:   CONTROLLER

Manufacturing defects and external disturbances degrade the performance of MEMS gyroscope [27]. It is difficult to get actual value of resonance frequency due to environmental effect which reduces the sensitivity of the gyroscope [28]. Neglecting these issues will lead to achieve wrong angular velocity [29]. These disturbances reduce the influence of the drive axis on the sense axis as well as the effect of Coriolis force. Hence, practical control techniques are very attractive research area in the field of MEMS gyroscopes [30].

Here, a sinusoidal signal is given in the drive direction to oscillate the proof mass (Figure 20) and the sensed signal (Figure 21). We can see here that output signal is not sinusoidal.
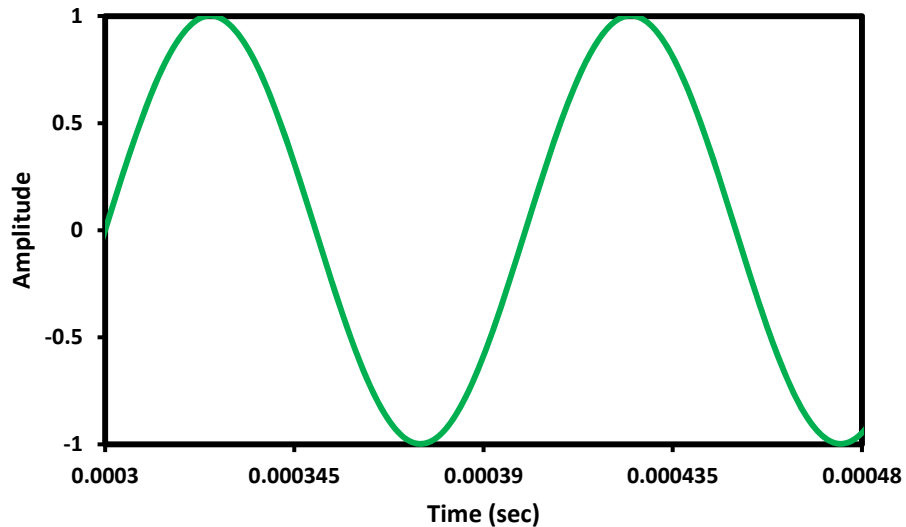
Figure 20: Input Signal (Drive Direction)
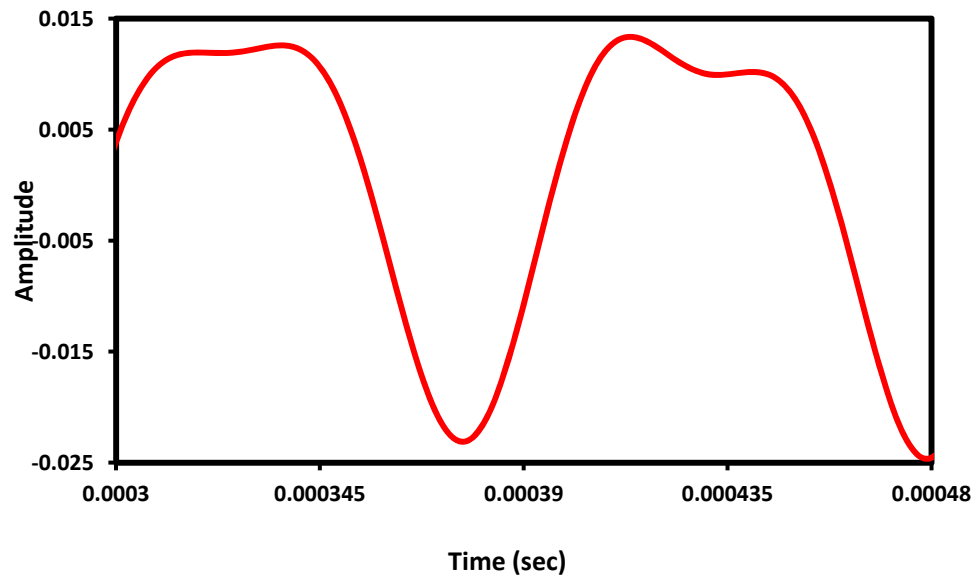
Figure 21: Output Signal (Sense Direction)
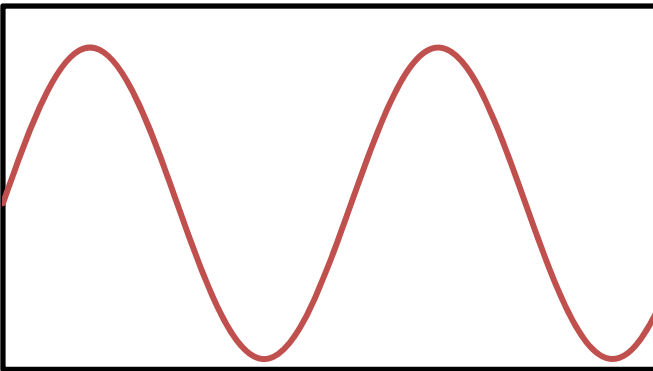
Figure 22: Hypothetical Input Signal
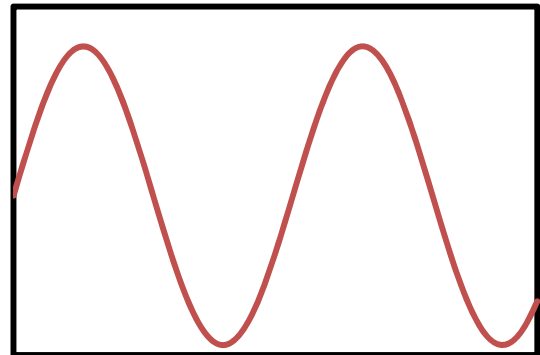
Figure 23: Hypothetical Expected Output Signal
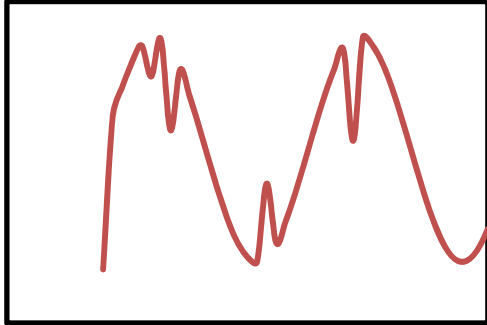
Figure 24: Hypothetical Actual Output Signal
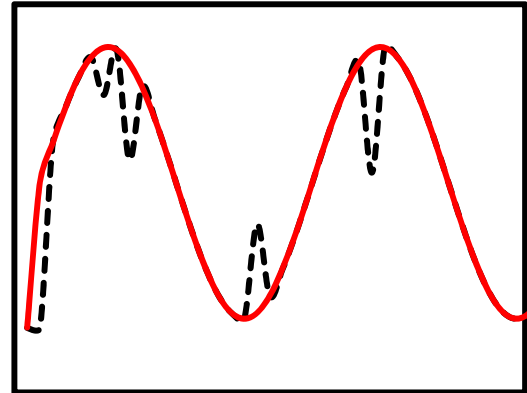
Figure 25: Hypothetical Repaired Signal by

using Controller

For example, this is a hypothetical input signal in the drive direction as shown in

Figure 22. This is the expected hypothetical output signal in the sense direction as shown in Figure 23. But due to manufacturing defects and environmental noises, we got the hypothetical distorted output signal in the sense direction as shown in Figure 24. Controller can repair the actual distorted output signal and bring it back to expected output signal as shown in Figure 25.

.

Choice of Controller

Depending on the applications and complexity, different types of controllers are

available.

PID controller

   PID controllers are very suitable for linear systems but practically don't produce the best results when the system is nonlinear [30]. When PID controller is used with other controller it can give highly accurate results [31].

Adaptive sliding mode controller

   Nonlinearities are always present in dynamic systems. Typical PID controller cannot handle these kind of nonlinearities. Adaptive controller can be used in these kind of situations because of its ability to adjust the parameters according to changing system dynamics. Robustness and insensitivity to external disturbances are notable features of adaptive controller. However, its requirements for extensive complex model structure discourages its use [32].

Neural controller:

   Neural network consists of neurons. Their connections are weighted. Relationship between neurons depends on their weighted sum of input and output [30]. Neural network can learn and approximate nonlinear functions even in uncertain situations [33]. The advantage of using neural control is that we need not to know the complex mathematical model [34].

Neuro Fuzzy Controller

   The neuro fuzzy systems inherit properties from both fuzzy systems and neural networks which take advantages of all the advantages of both fuzzy logic and neural

networks without all disadvantages [27]. A neuro-fuzzy system simultaneously work without precise mathematical model and can learn by itself [35]. When it is used for nonlinear systems, its robustness can almost avoid the external disturbances [36].
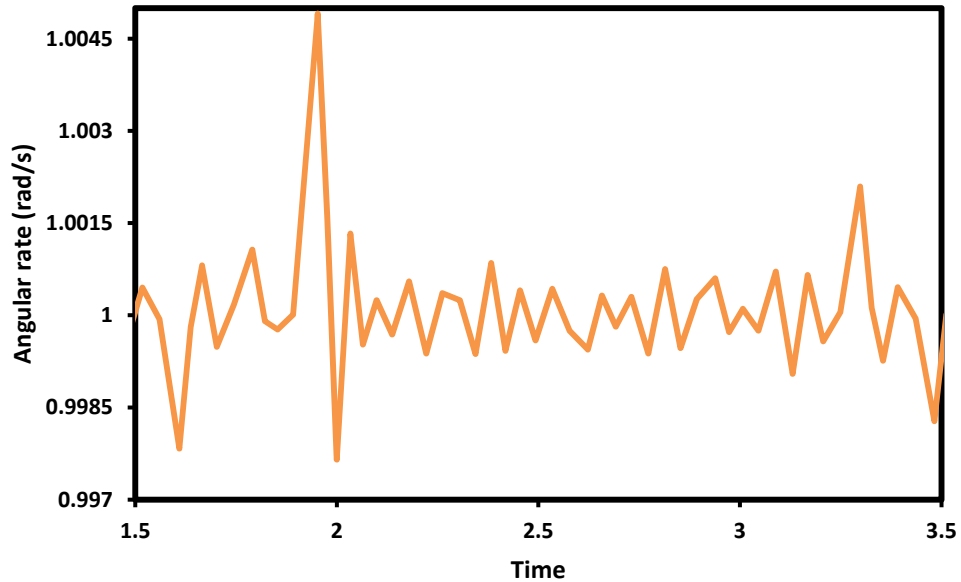
Figure 26: Noise without controller at 1 rad/s angular rate

Figure 26 shows the presence of noise in the sense output of gyroscope. For simplicity, a first order equation has been considered here. These noises make it difficult to read the actual sense signals. To reduce or eliminate the noises controllers are used. Here a continuous PID controller is used for noise reduction. Couples of trials have been made to tune the PID controller. Table 2, Figure 27, Figure 28 and Figure 29 show relevant data and figures. Peak time, peak value, rise time, slew rate, overshoot and undershoot parameters have been compared to get the tuned value.

Table 2: Signal characteristics for different P, I, D, N values

Trial	Parameters		Peak Time (sec)	Peak Value	Rise Time (ms)	Slew Rate(/s)	Overshoot (%)	Undershoot (%)
1	P	4	1.077	1.001	10.074	78.727	0.317	1.988
	I	200						
	D	0.04						
	F	21000						
2	P	8	1.07	1.001	4.610	171.950	-0.772	1.967
	I	400						
	D	0.08						
	F	28000						
3	P	12	1.068	1.001	2.983	265.630	-0.746	1.953
	I	600						
	D	0.12						
	F	35000						
4	P	16	1.067	1	2.204	359.441	-0.545	1.987
	I	800						
	D	0.16						
	F	42000						
5	P	20	1.066	1	1.748	453.284	-0.380	1.908
	I	1000						

	D	0.20						
	F	49000						
6	P	24	1.066	1	1.448	547.187	-2.252	1.971
	I	1200						
	D	0.24						
	F	49000						
7	P	2	1.907	1	14.909	53.123	0.083	1.993
	I	102						
	D	0.02						
	F	19747						
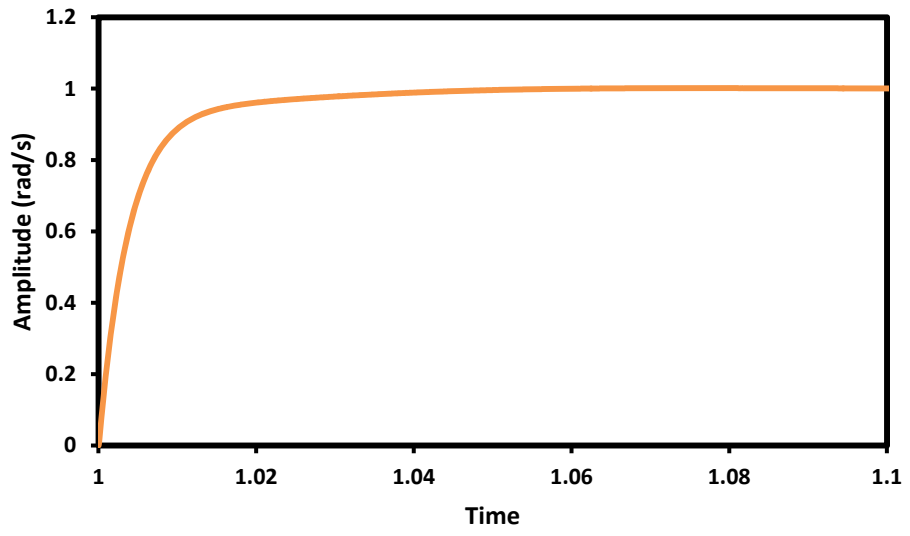
(Trial 1)
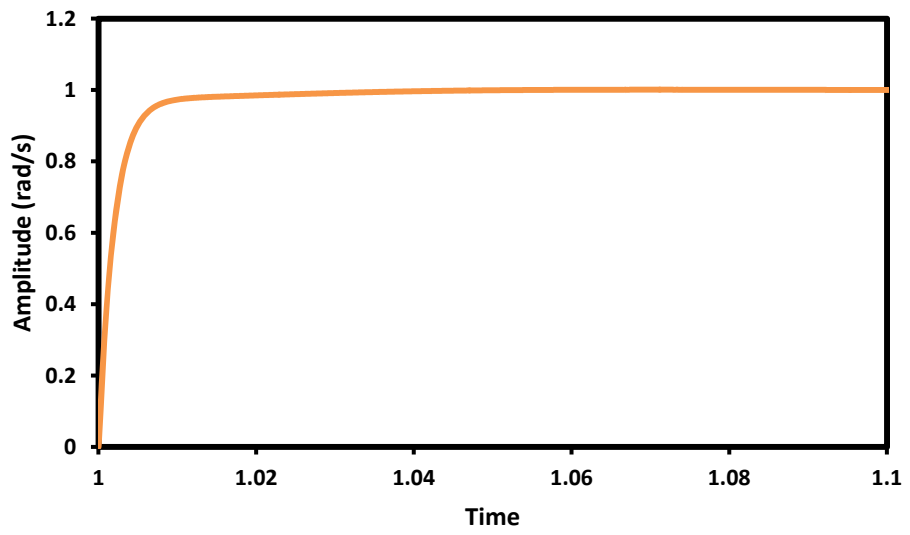
(Trial 2)
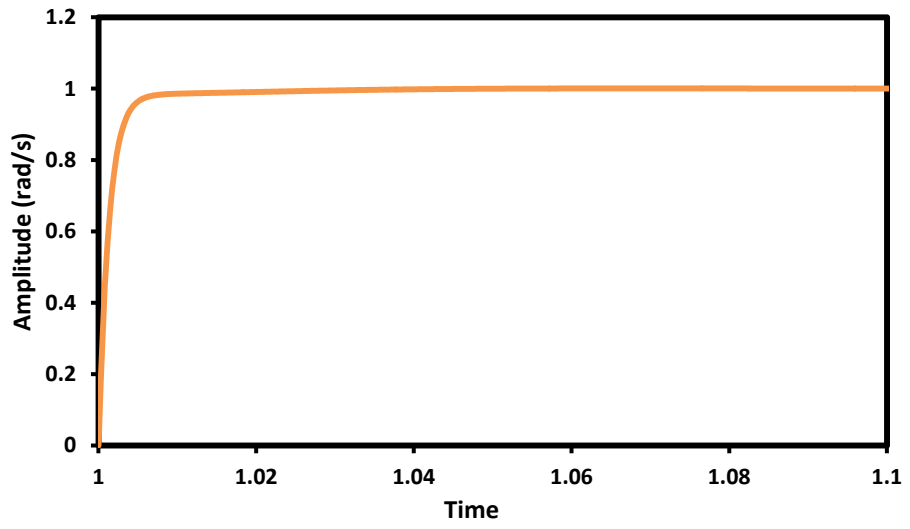
(Trial 3)
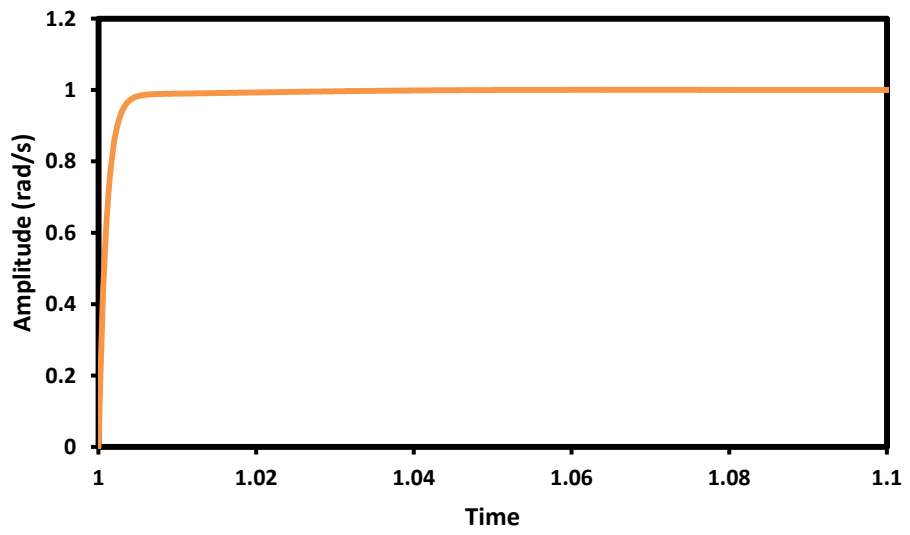
(Trial 4)
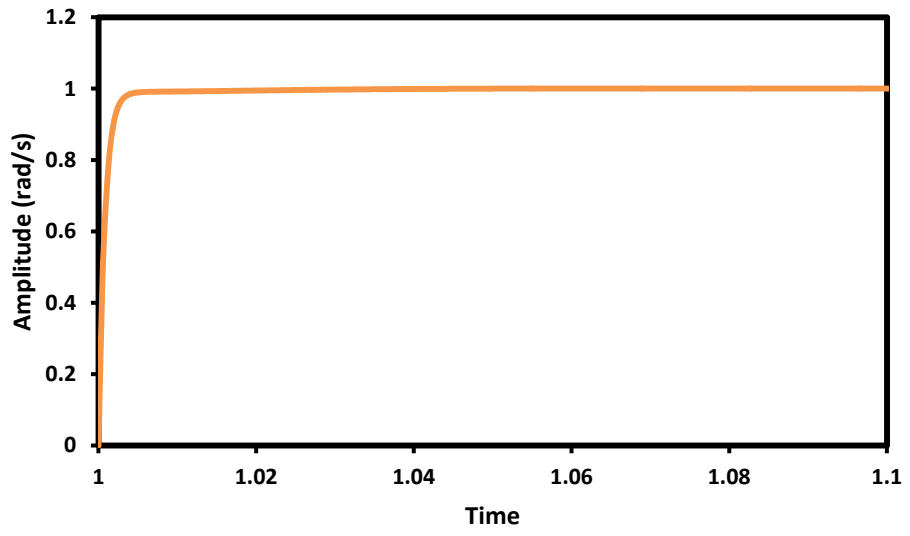
(Trial 5)
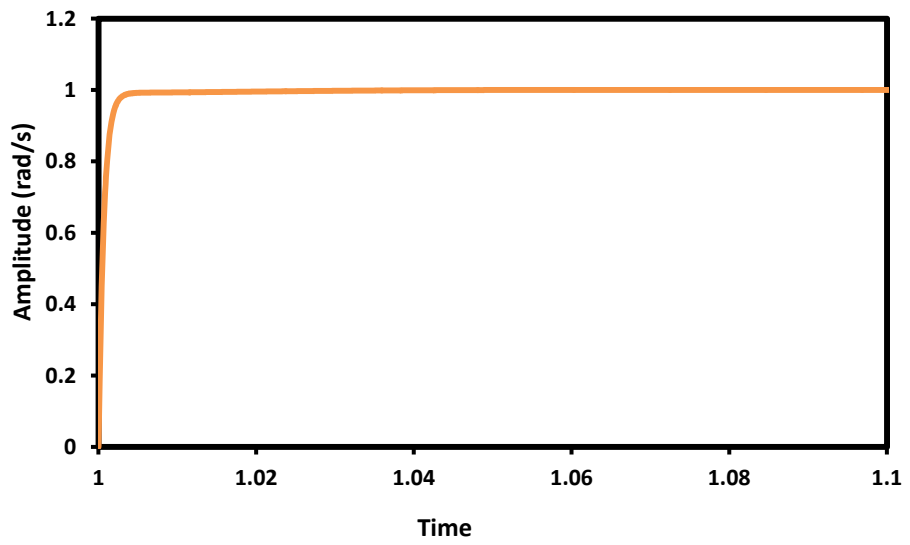
(Trial 6)
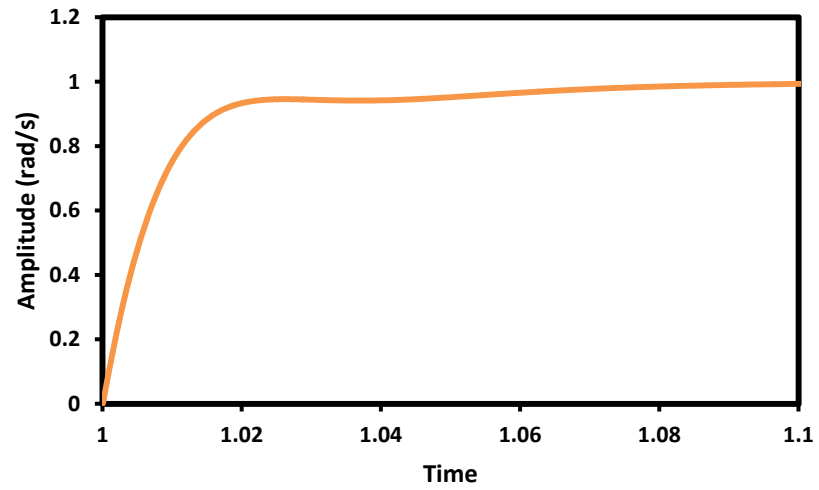
(Trial 7)

Figure 27: Step responses for different P, I, D, N values
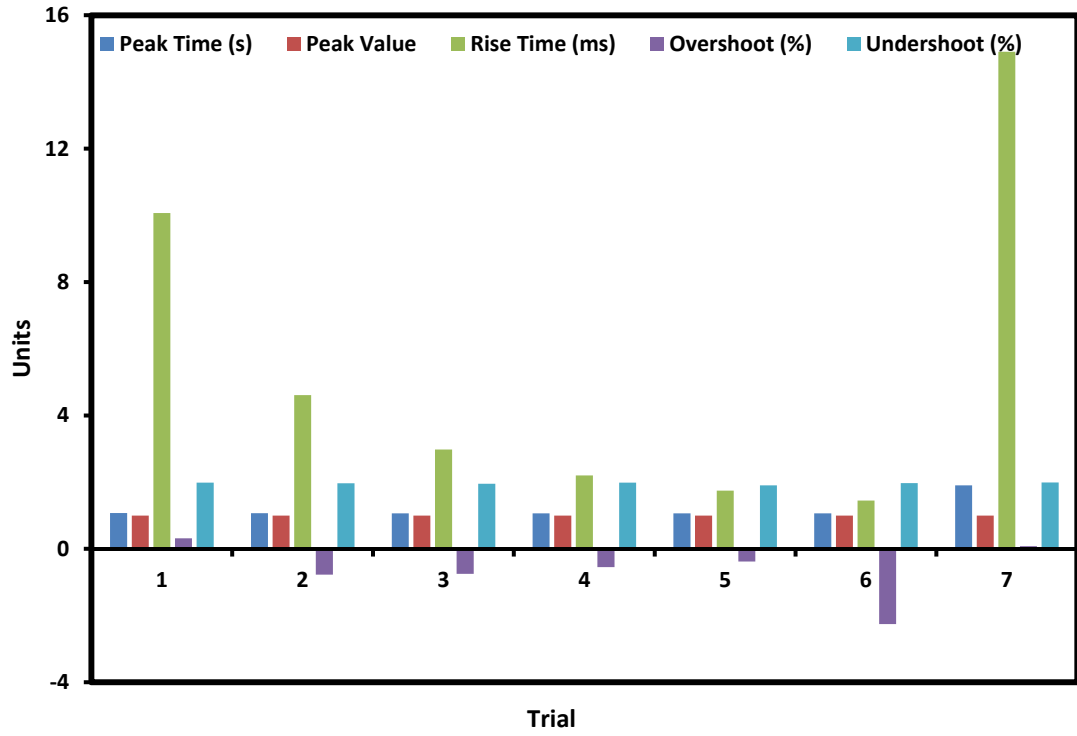
Figure 28: Signal characteristics for different P, I, D, N values
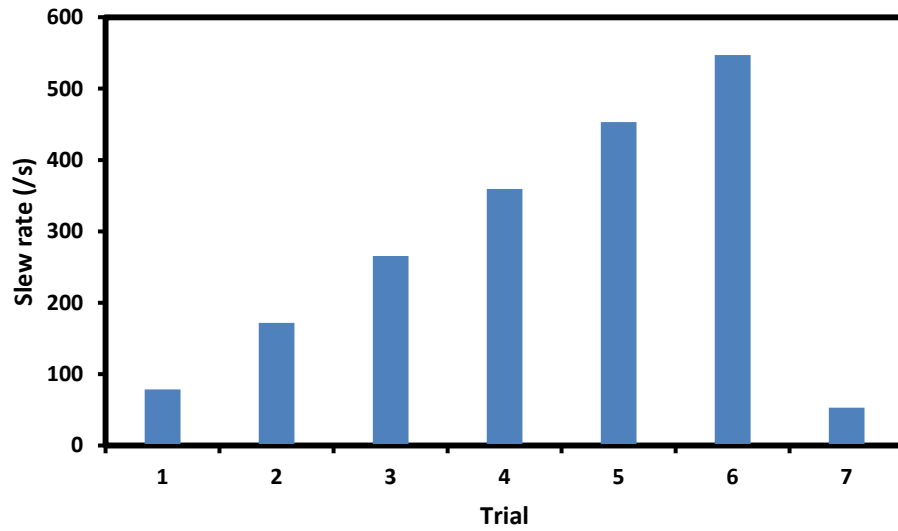
Figure 29: Slew rate
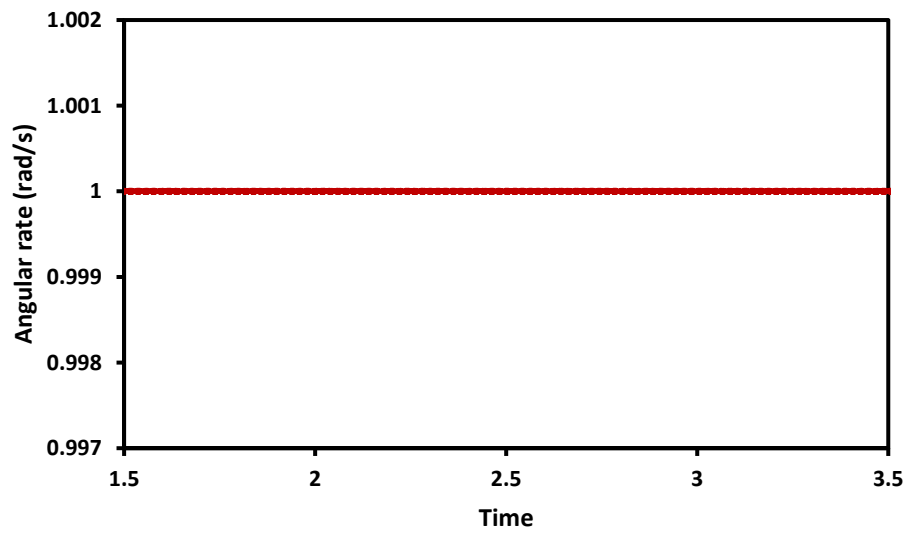
Figure 30: Noise reduced after using after continuous PID controller at 1 rad/s angular

rate

The continuous PID controller has been tuned using the values shown below:

Table 3: Continuous PID controller tuned parameters

Source	Values
Proportional (P)	3
Integrator (I)	102
Derivative (D)	0.02
Filter coefficient (N)	19747

Discrete PID controller also has been used for noise reduction (Figure 31).
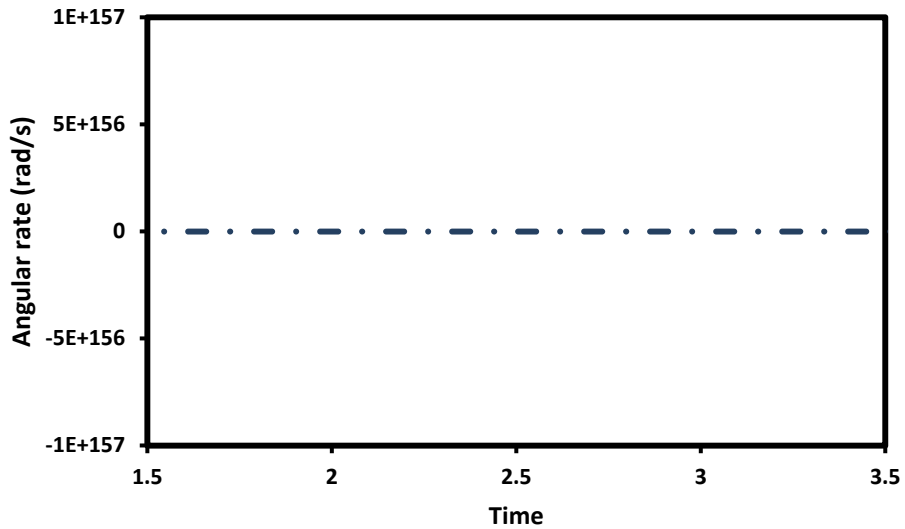
Figure 31: Noise reduced after using after discrete PID controller at 1 rad/s angular rate

The continuous PID controller has been tuned using the values shown below (Table 4):

Table 4: Discrete PID controller tuned parameters

Source	Values
Proportional (P)	3
Integrator (I)	102
Derivative (D)	0.02
Filter coefficient (N)	19747
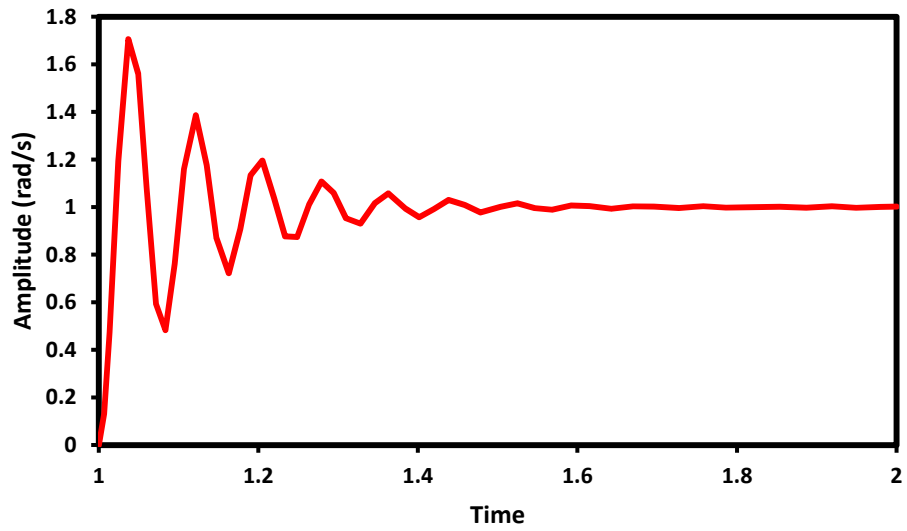
Figure 32: Unit step response without controller
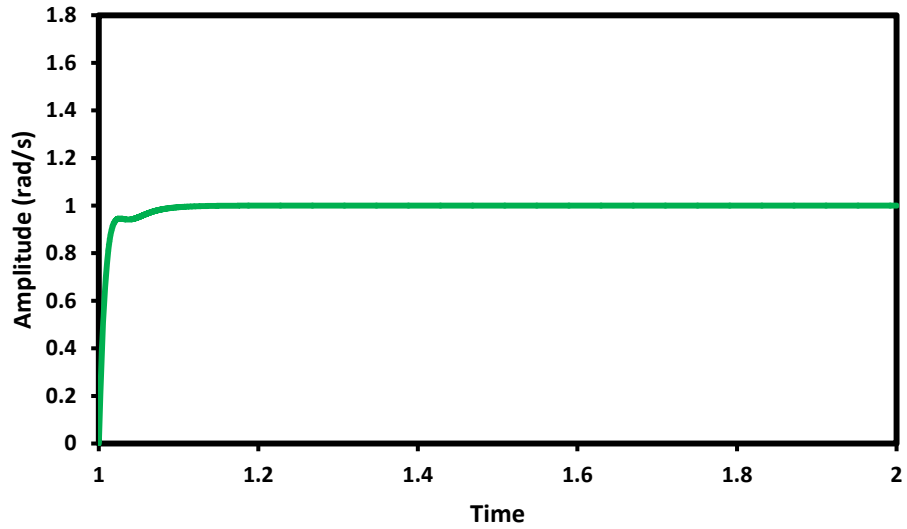
Figure 33: Unit step response with PID controller

Table 5: Comparison between without controller and PID controller at transient zone

	Without controller	PID controller
Rise Time (ms)	28.269	14.909
Slew Rate (/s)	28.046	53.123
Overshoot (%)	4.737	0.083
Undershoot (%)	-0.252	1.993
Peak Value	1.043	1
Peak Time (s)	1.056	1.907
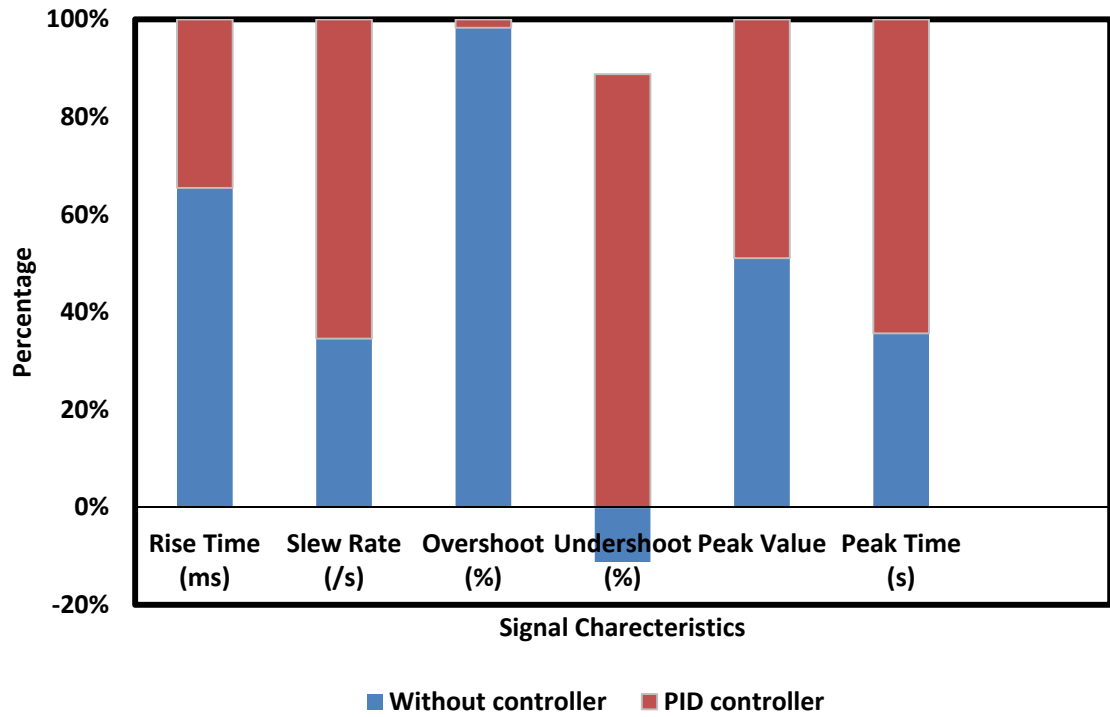
Figure 34: Comparison of signal characteristics between no controller and PID controller

CHAPTER 6:   CONCLUSION

This thesis investigates the effect of variation of suspending stiffness coefficients, damping coefficients and temperature on the performance of MEMS gyroscopes. Simulation results show how these parameters are affecting the error i.e. mismatch between the input and sense signals which will help to design appropriate system parameters as well as controllers to increase gyroscope accuracy. Simulation results also show that if stiffness in the sense direction remains constant at 71.62 N/m, stiffness in the drive direction is varied from 50% to 150%, the magnitudes at resonance frequencies show linear decreasing trend and amplitudes decrease as stiffness increases. However, decreasing the stiffness creates phase lag and distortion in output response. It is observed that if stiffness goes up by 50%, resonance frequency goes up by 21% and magnitude goes down by 27%. It has been observed that resonance frequency doesn't change that much with the change of sense mode stiffness. When damping increases to double, magnitude of resonance goes down by 10% and resonance frequency itself goes down by 0.16%. It is obvious from the simulations that the resonance frequencies do not change that much but the steepness of the slope decreases as drive mode damping increases after resonance frequencies. When the temperature is raised from -40°C to 60°C, stiffness goes down by 0.70 % and when the stiffness changes by 0.70 %, magnitude changes by 0.378 %. When the temperature is raised from -40°C to 60°C, damping is going up by 9.22 % and when the damping changes by 9.22 %, magnitude changes by 0.92 %.From the simulation result it is observed that

- Stiffness has the dominant effect on gyroscope accuracy.

- Temperature sensitivity can degrade resonance frequency and sense magnitude.

- Sense mode damping has little impact on the system.

- Changing weight of the proof mass and drive mode damping can moderately affect the magnitude of resonance frequency.

- It can be said that according to the result, by adjusting only stiffness, the system can be taken near optimum condition.

CHAPTER 7:   FUTURE WORK

In the future, it is planned to extend this by comparing these simulation results with the data obtained from physical experiments and implement an advanced controller like fuzzy logic to minimize the noise, rise time, undershoot, overshoot and maximize the gyroscope performance.

7.1   Why Fuzzy Logic Controller

Control system using fuzzy methodology can handle model uncertainties and manufacturing imperfections. The fuzzy controller can work even without any precise mathematical model [31]. The major limitations of Fuzzy Logic based controller are rules must be available, cannot learn by itself [34].

7.2   How does fuzzy controller work?

Fuzzy logic generally used in uncertain nonlinear systems. It consists of several steps. The general structure of a FLS is shown in Figure 35.
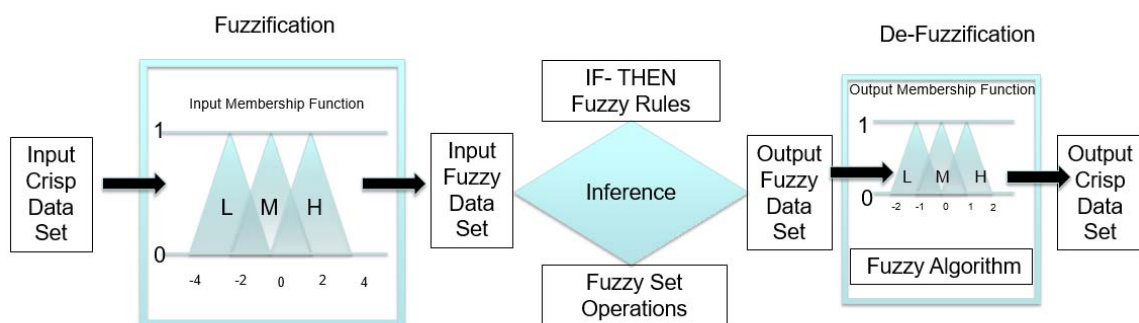
Figure 35: A Fuzzy Logic System

Fuzzy logic algorithm:

    1. Defining the linguistic variables

    2. Developing membership functions

    3. Developing rules

    4. Transforming input data to fuzzy data using the membership functions

    5. Getting the result from each rule

    6. Combining all the results

    7. Converting the combined result into non fuzzy data

Linguistic Variables

These are the variables whose values are natural words rather than numerical numbers. A linguistic variable is segregated into several linguistic terms.

Membership Functions

Membership converts the non-fuzzy input data to fuzzy linguistic values and vice versa. A fuzzy value can be the member of several sets at the same time. Different membership functions are available like triangular, trapezoidal, piecewise linear, Gaussian, singleton etc. [37].

Fuzzy Rules

Fuzzy rules control the output variable. A fuzzy rule consists of simple IF-THEN rule with a condition and a result.

Fuzzy Set Operations

The combination of fuzzy results are done by fuzzy set operations. If μ_A and μ_B are the membership functions for fuzzy sets A and B, Table 6 contains possible fuzzy operations for OR and AND. The operations for OR and AND operators are max and min. For NOT operation Equation 14 is used for fuzzy sets.

$$\mu_{\bar{A}}(x) = 1 - \mu_A(x) \qquad (14)$$

Table 6: Fuzzy Set Operations

	OR (Union)		AND (Intersection)
MAX	$\text{Max}(\mu_A(x), \mu_B(x))$	MIN	$\text{Min}((x), \mu_B(x))$
ASUM	$\mu_A(x) + \mu_B(x) - \mu_A(x)\mu_B(x)$	PROD	$\mu_A(x)\mu_B(x)$
BSUM	$\text{Min}(1, \mu_A(x) + \mu_B(x))$	BDIF	$\text{Max}(0, \mu_A(x) + \mu_B(x) - 1)$

Combining individual results in to a final result is called inference. Different methods are available for combining those results. Table 7 shows some methods for combining the results.

Table 7: Accumulation Methods

Operations	Formula
Maximum	$\text{Max}(\mu_A(x), \mu_B(x))$
Bounded Sum	$\text{Min}(1, \mu_A(x) + \mu_B(x))$
Normalized Sum	$\dfrac{\mu_A(x) + \mu_B(x)}{\text{Max}(1, \text{Max}(\mu_A(x'), \mu_B(x')))}$

Defuzzification

This step converts the resulted fuzzy value to normal or crisp data. Like Fuzzification, several Defuzzification methods are also available. The most popular ones are shown in in Table 8 [38].

Table 8: Defuzzification Algorithms & variables

Variable	Meaning	Operation	Formula
i	Index	Center of Gravity	$U = \dfrac{\int_{min}^{max} u\,\mu(u)\,du}{\int_{min}^{max} \mu(u)\,du}$
inf	Smallest value		
max	Upper limit of defuzzification		
min	Lower limit of defuzzification	Center of Gravity for Singletons	$\dfrac{\sum_{i=1}^{p}[u_i\mu_i]}{\sum_{i=1}^{p}[\mu_i]}$
p	Number of Singletons		
sup	Largest Value	Left Most Maximum	$U = inf(u'),\ \mu(u') = sup(\mu(u))$
u	Output Variable		
U	Result of Defuzzification	Right Most Maximum	$U = sup(u'),\ \mu(u') = sup(\mu(u))$
μ	Membership Function after accumulation		

REFERENCE

[1]   "IRE Standards on Navigation Aids: Definitions of Inertial Navigation Terms, 1962," 62 IRE 12.S1 (IEEE 174), pp. 1-6, 1962.

[2]   F. Braghin, F. Resta, E. Leo, and G. Spinola, "Nonlinear dynamics of vibrating MEMS," Sensors and Actuators A: Physical, vol. 134, pp. 98-108, 2007/02/28/ 2007.

[3]   J. Fei and C. Batur, "A novel adaptive sliding mode control with application to MEMS gyroscope," ISA Transactions, vol. 48, pp. 73-78, 2009/01/01/ 2009.

[4]   M. Wen, W. Wang, Z. Luo, Y. Xu, X. Wu, F. Hou, et al., "Modeling and analysis of temperature effect on MEMS gyroscope," in 2014 IEEE 64th Electronic Components and Technology Conference (ECTC), 2014, pp. 2048-2052.

[5]   J. Wang, S. Ban, and Y. Yang, "A Differential Self-Integration D-Dot Voltage Sensor and Experimental Research," IEEE Sensors Journal, vol. 15, pp. 3846-3852, 2015.

[6]   S. Woon-Tahk, S. Sangkyung, L. Jang Gyu, and K. Taesam, "Design and performance test of a MEMS vibratory gyroscope with a novel AGC force rebalance control," Journal of Micromechanics and Microengineering, vol. 17, p. 1939, 2007.

[7]   W. Juan and J. Fei, "Adaptive fuzzy approach for non-linearity compensation in MEMS gyroscope," Transactions of the Institute of Measurement and Control, vol. 35, pp. 1008-1015, 2013.

[8]   J. Collin, P. Davidson, M. Kirkko-Jaakkola, and H. Leppäkoski, "Inertial Sensors and Their Applications," in Handbook of Signal Processing Systems, S. S. Bhattacharyya, E. F. Deprettere, R. Leupers, and J. Takala, Eds., ed Cham: Springer International Publishing, 2019, pp. 51-85.

[9]   F. Khoshnoud and C. W. d. Silva, "Recent advances in MEMS sensor technology-mechanical applications," IEEE Instrumentation & Measurement Magazine, vol. 15, pp. 14-24, 2012.

[10]   "IEEE Standard Specification Format Guide and Test Procedure for Coriolis Vibratory Gyros," IEEE Std 1431-2004, pp. 1-78, 2004.

[11]   "IEEE Standard for Inertial Sensor Terminology," IEEE Std 528-2001, p. 0_1, 2001.

[12]   C. Acar and A. Shkel, MEMS Vibratory Gyroscopes: Structural Approaches to Improve Robustness (MEMS Reference Shelf): Springer Publishing Company, Incorporated, 2008.

[13]   M. Grewal and A. Andrews, "How Good Is Your Gyro [Ask the Experts]," IEEE Control Systems Magazine, vol. 30, pp. 12-86, 2010.

[14]   M. J. Ahamed, D. Senkal, A. A. Trusov, and A. M. Shkel, "Study of High Aspect Ratio NLD Plasma Etching and Postprocessing of Fused Silica and Borosilicate Glass," Journal of Microelectromechanical Systems, vol. 24, pp. 790-800, 2015.

[15]   J. Liu, J. Jaekel, D. Ramdani, N. Khan, D. S. K. Ting, and M. J. Ahamed, "Effect of Geometric and Material Properties on Thermoelastic Damping (TED) of 3D Hemispherical Inertial Resonator," p. V010T13A019, 2016.

[16] D. Senkal, M. J. Ahamed, M. H. A. Ardakani, S. Askari, and A. M. Shkel, "Demonstration of 1 Million Q-Factor on Microglassblown Wineglass Resonators With Out-of-Plane Electrostatic Transduction," Journal of Microelectromechanical Systems, vol. 24, pp. 29-37, 2015.

[17] A. M. Shkel, D. Senkal, and M. Ahamed, "METHOD OF FABRICATING MICRO-GLASSBLOWN GYROSCOPES," USA Patent US Patent US9702728B2, 2017.

[18] J. Fei and C. Batur, A novel adaptive sliding mode control with application to MEMS gyroscope vol. 48, 2008.

[19] W.-T. Sung, S. Sung, G.-I. Jee, and T. Kang, Design and performance test of a MEMS vibratory gyroscope with a novel AGC force rebalance control vol. 17, 2007.

[20] J. Fei, M. Xin, and W. Juan, Adaptive fuzzy sliding mode control using adaptive sliding gain for MEMS gyroscope vol. 35, 2013.

[21] Mathwork. (2018, 26 March). Simulink. Available: https:// www.mathworks.com /products/simulink.html

[22] J. Fei, W. Dai, M. Hua, and Y. Xue, "System Dynamics and Adaptive Control of MEMS Gyroscope Sensor," IFAC Proceedings Volumes, vol. 44, pp. 3551-3556, 2011/01/01/ 2011.

[23] M. R. Moghanni, J. Keighobadi, and A. Ghanbari, "Fuzzy Adaptive Sliding Mode Controller for MEMS Vibratory Rate Gyroscope," IFAC Proceedings Volumes, vol. 44, pp. 4192-4197, 2011/01/01/ 2011.

[24]   R. Horowitz, New Adaptive Mode of Operation for MEMS Gyroscopes vol. 126, 2004.

[25]   M. L. C. d. Laat, H. H. P. Garza, J. L. Herder, and M. K. Ghatkesar, "A review on in situ stiffness adjustment methods in MEMS," Journal of Micromechanics and Microengineering, vol. 26, p. 063001, 2016.

[26]   J. Fei and H. Ding, "System Dynamics and Adaptive Control for MEMS Gyroscope Sensor," International Journal of Advanced Robotic Systems, vol. 7, p. 29, 2010/12/01 2010.

[27]   J. Fei and J. Zhou, "Robust Adaptive Control of MEMS Triaxial Gyroscope Using Fuzzy Compensator," IEEE Transactions on Systems, Man, and Cybernetics, Part B (Cybernetics), vol. 42, pp. 1599-1607, 2012.

[28]   M. Fazlyab, M. Z. Pedram, H. Salarieh, and A. Alasty, "Parameter estimation and interval type-2 fuzzy sliding mode control of a z-axis MEMS gyroscope," ISA Transactions, vol. 52, pp. 900-911, 2013/11/01/ 2013.

[29]   R. Zhang, T. Shao, W. Zhao, A. Li, and B. Xu, Sliding Mode Control of MEMS Gyroscopes Using Composite Learning vol. 275, 2017.

[30]   T. T. Xie, H. Yu, and B. M. Wilamowski, "Comparison of Fuzzy and Neural Systems for Implementation of Nonlinear Control Surfaces," in Human – Computer Systems Interaction: Backgrounds and Applications 2: Part 2, Z. S. Hippe, J. L. Kulikowski, and T. Mroczek, Eds., ed Berlin, Heidelberg: Springer Berlin Heidelberg, 2012, pp. 313-324.

[31]   F. Gouadria, L. Sbita, and N. Sigrimis, "Comparison between self-tuning fuzzy PID and classic PID controllers for greenhouse system," in 2017 International Conference on Green Energy Conversion Systems (GECS), 2017, pp. 1-6.

[32]   J. Fei and H. Ding, "Adaptive sliding mode control of dynamic system using RBF neural network," Nonlinear Dynamics, vol. 70, pp. 1563-1573, 2012/10/01 2012.

[33]   R. Zhang, T. Shao, W. Zhao, A. Li, and B. Xu, "Sliding mode control of MEMS gyroscopes using composite learning," Neurocomputing, vol. 275, pp. 2555-2564, 2018/01/31/ 2018.

[34]   M. Nagai, A. Moran, Y. Tamura, and S. Koizumi, "Identification and control of nonlinear active pneumatic suspension for railway vehicles, using neural networks," Control Engineering Practice, vol. 5, pp. 1137-1144, 1997/08/01/ 1997.

[35]   T. R. Kiran and S. P. S. Rajput, "An effectiveness model for an indirect evaporative cooling (IEC) system: Comparison of artificial neural networks (ANN), adaptive neuro-fuzzy inference system (ANFIS) and fuzzy inference system (FIS) approach," Applied Soft Computing, vol. 11, pp. 3525-3533, 2011/06/01/ 2011.

[36]   W. Yan, S. Hou, Y. Fang, and J. Fei, "Robust adaptive nonsingular terminal sliding mode control of MEMS gyroscope using fuzzy-neural-network compensator," International Journal of Machine Learning and Cybernetics, vol. 8, pp. 1287-1299, 2017/08/01 2017.

[37]   C. Byoung-doo, P. Sangjun, K. Hyoungho, P. Seung-Joon, P. Yonghwa, L. Geunwon, et al., "The first sub-deg/hr bias stability, silicon-microfabricated gyroscope," in The 13th International Conference on Solid-State Sensors, Actuators

and Microsystems, 2005. Digest of Technical Papers. TRANSDUCERS '05., 2005, pp. 180-183 Vol. 1.

[38]   J. M. Mendel, "Fuzzy logic systems for engineering: a tutorial," Proceedings of the IEEE, vol. 83, pp. 345-377, 1995.

VITA AUCTORIS

NAME: Md. Imrul Kaes

PLACE OF BIRTH: Dhaka, Bangladesh

YEAR OF BIRTH: 1985

EDUCATION: Bachelor in science in industrial & production engineering, Bangladesh University of Engineering & Technology, Dhaka, Bangladesh.

Master of engineering in industrial engineering, University of Windsor, Windsor, ON, Canada.